The Astrophysical Journal Supplement Series, 232:3 (22pp), 2017 September https://doi.org/10.3847/1538-4365/aa8098

Deep, Broadband Spectral Line Surveys of Molecule-rich Interstellar Clouds

Susanna L. Widicus Weaver[1], Jacob C. Laas[1,5], Luyao Zou[1], Jay A. Kroll[1,6], Mary L. Rad[1], Brian M. Hays[1], James L. Sanders[1], Dariusz C. Lis[2,3], Trevor N. Cross[1], Nadine Wehres[1,7], Brett A. McGuire[1,4,8], and Matthew C. Sumner[2,9]
[1] Department of Chemistry, Emory University, Atlanta, GA 30322, USA; susanna.widicus.weaver@emory.edu
[2] California Institute of Technology, Cahill Center for Astronomy and Astrophysics 301-17, Pasadena, CA 91125, USA
[3] LERMA, Observatoire de Paris, PSL Research University, CNRS, Sorbonne Universités, UPMC Univ. Paris 06, F-75014, Paris, France
[4] National Radio Astronomy Observatory, 520 Edgemont Road, Charlottesville, VA 22903-2475, USA
Received 2017 May 2; revised 2017 June 30; accepted 2017 July 13; published 2017 August 22

Abstract

Spectral line surveys are an indispensable tool for exploring the physical and chemical evolution of astrophysical environments due to the vast amount of data that can be obtained in a relatively short amount of time. We present deep, broadband spectral line surveys of 30 interstellar clouds using two broadband $\lambda = 1.3$ mm receivers at the Caltech Submillimeter Observatory. This information can be used to probe the influence of physical environment on molecular complexity. We observed a wide variety of sources to examine the relative abundances of organic molecules as they relate to the physical properties of the source (i.e., temperature, density, dynamics, etc.). The spectra are highly sensitive, with noise levels $\leqslant$25 mK at a velocity resolution of $\sim$0.35 km s^{-1}. In the initial analysis presented here, column densities and rotational temperatures have been determined for the molecular species that contribute significantly to the spectral line density in this wavelength regime. We present these results and discuss their implications for complex molecule formation in the interstellar medium.

Key words: astrochemistry – ISM: abundances – ISM: clouds – ISM: molecules

Supporting material: data behind figure, figure set, machine-readable table

1. Introduction

Nearly 200 molecules have been detected in interstellar and circumstellar environments (Müller et al. 2001, 2005; CDMS 2017), and a great fraction of these are complex organic molecules (COMs). Here, following the convention of Herbst & van Dishoeck (2009), we define a COM as a molecule containing six or more atoms. Laboratory, observational, and modeling studies have revealed that very little is understood about the chemical and physical mechanisms driving complex molecule formation in the interstellar medium (ISM). Calculations (Horn et al. 2004) and laboratory results (Geppert et al. 2006) have shown that the textbook chemical mechanisms thought to lead to complex organics in the ISM—ion–molecule and electron recombination reactions—are actually inefficient processes for the formation of most complex molecules. Even the ubiquitous molecule methanol presents a challenge. Ion–molecule reactions account for only a small percentage of the methanol observed in dense clouds, and neutral methanol comprises only $\sim$3% of the dissociative recombination products from protonated methanol (Geppert et al. 2006).

Conversely, chemical modeling suggests that reactions of simple radicals on interstellar grain surfaces may be integral to COM formation (Garrod et al. 2008; Laas et al. 2011), and that grain-surface reactions are the dominant formation mechanism for many of the most abundant COMs under typical interstellar cloud conditions. Based on this type of chemistry, many other previously undetected COMs are also predicted to be present in high abundance in hot cores. Modeling studies must be compared with observations to test their robustness. Unfortunately, the subset of sources for which extensive COM inventories have been compiled is quite small. Therefore, the modeling studies have primarily focused on comparisons with the Sagittarius B2(N) hot molecular core, which has the highest number of detected molecules of any sightline studied to date (Snyder 2006), but may not be representative of all sources.

Before a full understanding of interstellar organic chemistry can be obtained, we must test these models against observations to gain a comprehensive view of the possible chemical and physical parameter space. Previously, molecular observations largely consisted of targeted searches focusing on a few lines of only the most abundant molecules, or on molecules that were high-priority targets. Unbiased, self-consistent, broadband spectral line surveys, however, are more effective in determining the true composition of interstellar clouds as they allow the acquisition of spectral data over large frequency ranges and sample many transitions of each molecule. It has already been shown through the initial results reported from the Atacama Large Millimeter/Submillimeter Array (ALMA) that more COMs will be detected in all interstellar environments as spectral sensitivity, spectral bandwidth, and spatial resolution continue to increase. Therefore, such broadband surveys in the millimeter band will guide observations at higher frequencies with ALMA and other submillimeter and far-IR telescopes by identifying the sources that have the richest chemical inventory.

We present here the first results from our molecular line survey observations using two broadband $\lambda = 1.3$ mm receivers at the Caltech Submillimeter Observatory (CSO). The goal

[5] Current address: Max-Planck-Institut für extraterrestrische Physik (MPE), Gießenbachstraße 1, D-85741 Garching, Germany.
[6] Current address: University of Colorado, Department of Chemistry and Biochemistry, UCB 215, Boulder, CO 80309, USA.
[7] Current address: I. Physikalisches Institut, Universität zu Köln, Zülpicher Str. 77, D-50937 Köln, Germany.
[8] B.A.M. is a Jansky Fellow of the National Radio Astronomy Observatory. The National Radio Astronomy Observatory is a facility of the National Science Foundation operated under cooperative agreement by Associated Universities, Inc.
[9] Current address: Sandia National Laboratories, PO Box 969, Livermore, CA 94551-0969.

of this program is to conduct deep, broadband spectral line surveys of interstellar clouds to probe the influence of the physical environment on molecular complexity. We are observing a wide variety of sources in an attempt to correlate the relative abundances of organic molecules with the physical properties of the source (i.e., temperature, density, dynamics, etc.). Our broader research goal is to improve astrochemical models to the point where accurate predictions of complex molecular inventory can be made based on the physical and chemical environment of a given source. The information gained from our observations will serve as a benchmark for these astrochemical models, and therefore will hold the promise of significantly advancing our understanding of interstellar chemical processes. We report here on the details of the observations, the spectral analysis process, and the initial results for the molecular species that contribute significantly to the spectral line density in this spectral regime.

2. Observations and Data Reduction

The observations were performed with the 10.4 m Leighton Telescope of the CSO[10] between 2007 September and 2013 June. The nominal source positions and values assumed for $v_{\rm lsr}$ are listed in Table 1. Typical system temperatures ($T_{\rm sys}$) during the observations were <400 K; $T_{\rm sys}$ was higher during periods of high opacity, but did not exceed 1100 K.

Observations were performed using two sets of receivers and spectrometers. The first was a prototype 230 GHz wideband receiver (Rice et al. 2003; Kaul et al. 2004; Sumner 2011), which was used with the facility acousto-optical spectrometer (AOS; Horn et al. 1999). The receiver has a 12 GHz bandwidth, but the total IF bandwidth for the observations was limited by the AOS to 4 GHz, with a channel width of ∼0.65 MHz. The second receiver was the facility 230 GHz wideband receiver (Kooi et al. 2007), used with the facility Fast Fourier Transform Spectrometer (Klein et al. 2006). The receiver is a dual-frequency, tunerless wide-IF bandwidth (4–8 GHz) system with a fully synthesized LO; the total IF bandwidth for the observations was 4 GHz, with a channel width of ∼0.27 MHz, which is equivalent to a velocity resolution of ∼0.35 km s^{-1}.

All collected spectra were double sideband (DSB). A set of rest frequencies in the range 223.192–251.192 GHz was chosen, with each rest frequency setting being separated by 4 GHz. Each frequency point was sampled with a minimum redundancy of six to ensure sufficient sampling for deconvolution of the DSB spectra; most frequencies were sampled with a redundancy of eight. To achieve this redundancy, four IF offsets (4.254, 5.268, 6.754, and 7.795 GHz) were applied to each rest frequency, and DSB spectra were collected at each of these frequency settings. Additional IF offsets of 4.753, 6.283, 5.767, and 7.269 GHz were applied to the two lowest rest frequency settings. The number of DSB spectra acquired for each source varied, depending on weather conditions and the amount of available observing time.

Spectral intensities for the raw data were calibrated using the standard chopper wheel calibration method and placed on the atmosphere-corrected temperature scale, T_a^*. The chopper settings used were either 70″ ± 8″ of throw with a chopping frequency of 1.123 Hz, or 90″ ± 8″ of throw with a chopping frequency of 1.1 Hz. The estimated percent calibration error in antenna temperature is <20%, based on previous experience with this hardware. Integration times were adjusted based on the $T_{\rm sys}$ determined after tuning the receiver to a given frequency setting (i.e., for one set of rest frequency and IF values), such that the noise level achieved for a given frequency setting was ∼30 mK. Pointing was verified on average every two hours, and pointing offsets were consistent to within ⩽5″ over the course of a given night. As an independent verification of the pointing accuracy, each spectrum was checked against previous spectra recorded for consistency in spectral line intensity. The full-width-half-power beam size at 230 GHz was determined to be 33.″4 for the prototype receiver, and 35.″5 for the facility receiver.

Spectral cleaning and deconvolution were performed using the CLASS software package (versions jun13a and jul14a) included in the GILDAS suite of programs (Institut de Radioastronomie Millimétrique, Grenoble, France; GILDAS 2017). Baselines were fitted and removed from each DSB spectrum using a linear function for most sources. A small number of the sources required more complicated baseline fitting via boxcar averaging or interpolating a low-order polynomial. In cases where the line density precluded a reliable baseline fit, a constant offset was subtracted from the T_a^* scale. This offset was determined through comparison to the baseline in neighboring spectral windows. In general, the baselines were adjusted until they were as close as possible to zero. The process was checked for reproducibility, and the noise that was introduced was comparable to or less than the overall noise level of the spectra. In addition to baseline subtraction, some spurious noise features were present in the spectra, but their identification was straightforward because they were significantly narrower than the spectral line widths. Such noise features were removed from the spectra by blanking the affected channels prior to processing. After baseline subtraction and removal of noise features, the spectra were resampled at a uniform channel spacing of 1 MHz. The deconvolution was performed using the standard routine included in CLASS. An initial deconvolution was performed assuming no gain variations between the upper and lower sidebands. This was then used as an initial guess to constrain a second deconvolution allowing for varying gains between sidebands. Due to the nature of the algorithm used, extremely strong lines in the spectrum can produce ghosts visible above the final residual noise. Therefore, the CO line at 230.5 GHz and other strong spectral features with intensities above 2 K were masked during deconvolution and later stitched back into the spectrum to prevent the introduction of spurious features. After deconvolution was completed, it was found that a few strong features in the image sideband produced spectral artifacts appearing as ghosts, that manifest as negative features in the deconvolved spectrum. These features were blanked in the deconvolved spectrum. After deconvolution, all intensities were corrected to the main beam temperature scale, $T_{\rm mb}$, using the relation $T_{\rm mb} = T_a^*/\eta_{\rm mb}$. Here, $\eta_{\rm mb}$ is the main beam efficiency, which was determined through observation of planets to be 57% ± 10% for both receivers. The root-mean-squared noise in the deconvolved spectra was determined to be ⩽25 mK on the $T_{\rm mb}$ scale.

3. Line Identification and Analysis

The deconvolved spectra are broadband, highly sensitive, chemically complex, and line-blended in many cases. Detailed spectral analysis using the traditional Boltzmann diagram approach was therefore challenging. Such analyses are often unreliable because they are conducted one molecule at a time

[10] The CSO was operated by the California Institute of Technology under contract from the National Science Foundation.

Table 1
Sources, Positions, and Velocities Used in the Observations, and Source Physical Parameters

Source Name	Source Type	α (J2000)	δ (J2000)	v_{lsr} (km s^{-1})	Distance (pc)	Luminosity ($L_\odot$)	Mass (Gas and Dust) ($M_\odot$)	References
W3(H_2O)	Hot Core	$2^h27^m04\overset{s}{.}61$	+61°52′25 0″	−47.0	2040	$>10^5$	26	1, 2
L1448 MM-1	Class 0 + Outflow	$3^h25^m38\overset{s}{.}80$	+30°44′05 0″	0.0	232	11.6	<2	3–5
NGC 1333 IRAS 2A	Hot Corino	$3^h28^m55\overset{s}{.}40$	+31°14′35 0″	7.8	235	20.7	0.12	4, 6, 7
NGC 1333 IRAS 4A	Hot Corino	$3^h29^m10\overset{s}{.}30$	+31°13′31 0″	6.8	235	7.7	1.1	4, 6, 7
NGC 1333 IRAS 4B	Hot Corino	$3^h29^m11\overset{s}{.}99$	+31°13′08 9″	5.0	235	7.7	0.56	4, 6, 7
B1-b	Class 0	$3^h33^m20\overset{s}{.}80$	+31°07′40 0″	0.39	230	<3	∼1.5	8
Orion-KL	Hot Core	$5^h35^m14\overset{s}{.}16$	−05°22′21 5″	8.0	500	$>10^5$	10	9, 10
NGC 2264	Hot Core	$6^h41^m12\overset{s}{.}00$	+9°29′09 0″	7.6	800	71 − 102	48	11–13
NGC 6334–29	Class 0	$17^h19^m57\overset{s}{.}00$	−35°57′51 0″	−5.0	1.7 k	1.7×10^5	<200	14–16
NGC 6334–38	Class 0	$17^h20^m18\overset{s}{.}00$	−35°54′42 0″	−5.0	1.7 k	$<2 \times 10^5$	<175	14–16
NGC 6334–43	Class 0	$17^h20^m23\overset{s}{.}00$	−35°54′55 0″	−2.6	1.7 k	$<2 \times 10^5$	<150	14–16
NGC 6334-I(N)	Class 0	$17^h20^m55\overset{s}{.}00$	−35°45′40 0″	−2.6	1.7 k	5×10^4	<500	14, 15, 17
Sgr B2(N-LMH)	Hot Core	$17^h47^m19\overset{s}{.}89$	−28°22′19 3″	64	8.5 k	6×10^6	>2000	9
GCM+0.693-0.027	Shocked Region	$17^h47^m21\overset{s}{.}86$	−28°21′27 1″	68.0	[a]	[a]	[a]	
GAL 10.47+00.03	Hot Core	$18^h08^m38\overset{s}{.}40$	−19°51′51 8″	67.8	10.8 k	$\sim 3 \times 10^5$	2200	9, 18, 19
GAL 12.21–0.10	H II Region	$18^h12^m39\overset{s}{.}70$	−18°24′20 9″	24.0	13.5 k	$<10^6$	<14000	18, 20, 21
GAL 12.91–00.26	Hot Core	$18^h14^m39\overset{s}{.}00$	−17°52′0. 0″	37.5	13.6 k	10^5	>70	18, 22, 23
HH 80–81	Outflow	$18^h19^m12\overset{s}{.}30$	−20°47′27 5″	12.2	1.9 k	$\sim 2.4 \times 10^6$	>10	24, 25
GAL 19.61–0.23	Hot Core	$18^h27^m37\overset{s}{.}99$	−11°56′42 0″	40.0	12.0 k	$<2 \times 10^5$	450	9, 18, 20
G24.33+00.11 MM1	Hot Core	$18^h35^m08\overset{s}{.}14$	−7°35′01 1″	113.4	6.3 k	$\sim 5 \times 10^4$	26	26
GAL 24.78+0.08	Hot Core	$18^h36^m12\overset{s}{.}60$	−7°12′11 0″	111.0	6.1 k	$<2 \times 10^5$	250	18, 21, 27
GAL 31.41+0.31	Hot Core	$18^h47^m34\overset{s}{.}61$	−1°12′42 8″	97.0	7.9 k	$\sim 2 \times 10^5$	∼2000	28, 29
GAL 034.3+00.2	Hot Core	$18^h53^m18\overset{s}{.}54$	+1°14′57 9″	58.0	3.7 k	$\sim 9 \times 10^4$	7000	30, 31
GAL 45.47+0.05	Hot Core	$19^h14^m25\overset{s}{.}60$	+11°09′26 0″	62.0	8.0 k	$\sim 1 \times 10^6$	250	9, 32
W51	Hot Core	$19^h23^m43\overset{s}{.}50$	+14°30′34 0″	55.0	5.4 k	$<5 \times 10^5$	∼250	21, 33, 34
GAL 75.78+0.34	H II Region	$20^h21^m44\overset{s}{.}09$	+37°26′39 8″	4.0	3.83	$<3 \times 10^4$	<100	35, 36
W75N	Hot Core	$20^h38^m36\overset{s}{.}60$	+42°37′32 0″	10.0	1.7 k	$<5 \times 10^4$	<2	20, 37, 38
DR21(OH)	Hot Core	$20^h39^m01\overset{s}{.}10$	+42°22′49 1″	−3.0	3.0 k	5×10^4	350	9
L1157 B1	Class 0 + Outflow	$20^h39^m10\overset{s}{.}20$	+68°01′11 5″	2.7	325	5.8	0.2	7, 39, 40
NGC 7538	Hot Core	$23^h13^m45\overset{s}{.}70$	+61°28′21 0″	−57.0	2.8 k	2×10^4	<2000	41–43

Note.
[a] This source has not been well-characterized.

References. (1) Qin et al. (2015), (2) Wyrowski et al. (1999b), (3) Hirota et al. (2011), (4) van Dishoeck et al. (2011), (5) Tobin et al. (2015), (6) Hirota et al. (2008), (7) Jørgensen et al. (2007), (8) Öberg et al. (2010), (9) Kurtz et al. (2000), (10) McKee & Tan (2003), (11) Raimond (1966), (12) Cunningham et al. (2016), (13) Ward-Thompson et al. (2000), (14) Neckel (1978), (15) Loughran et al. (1986), (16) Matthews et al. (2008), (17) Gezari (1982), (18) Pandian et al. (2008), (19) Cesaroni et al. (2010), (20) Wu et al. (2010), (21) Ginsburg et al. (2012), (22) Faúndez et al. (2004), (23) Galván-Madrid et al. (2010), (24) Maud et al. (2015), (25) Fernández-López et al. (2011), (26) Rathborne et al. (2011), (27) Beltrán et al. (2004), (28) Le Teuff et al. (2000), (29) Cesaroni et al. (2010), (30) Wood & Churchwell (1989), (31) Mookerjea et al. (2007), (32) Hernández-Hernández et al. (2014), (33) Sato et al. (2010), (34) Shi et al. (2010) (35) Sánchez-Monge et al. (2013), (36) Pipher et al. (1979), (37) Schneider et al. (2006), (38) Minh et al. (2010), (39) Straizys et al. (1992), (40) Shirley et al. (2000), (41) Crampton et al. (1978), (42) Willner (1976), (43) Werner et al. (1979).

using a small set of lines for which line widths are determined independently and do not account for possible line blending. We have therefore developed a new program that analyzes all of the lines from one molecule across the entire broadband spectrum simultaneously. This Global Optimization and Broadband Analysis Software for Interstellar Chemistry (GOBASIC) is described in detail elsewhere (Rad et al. 2016). The performance of this software has been previously benchmarked (Rad et al. 2016) against both synthetic spectra and through a comparison between our Orion-KL data set and the results of Blake et al. (1986), and has been found to reliably model line surveys such as those considered here. In short, the software assumes local thermodynamic equilibrium (LTE) and Gaussian line shapes, and conducts a simultaneous, multi-molecule, multicomponent, broadband spectral analysis. It is worthwhile to note that the rotational temperatures of molecules from this LTE analysis are not guaranteed to be the true gas kinetic temperatures. Rather, it only means that the molecular line emission can be modeled by a single excitation temperature under Boltzmann statistics. We used published line surveys for Sgr B2(N) (Nummelin et al. 1998a) and Orion-KL (Sutton et al. 1985; Blake et al. 1986, 1987) to guide the initial list of molecules that were included for the analysis of this data set. We imported spectral line catalogs from the Cologne Database for Molecular Spectroscopy (CDMS; Müller et al. 2005) and the Jet Propulsion Laboratory (JPL) Spectral Line Catalog (Pickett et al. 1998). Unless combined in the JPL/CDMS catalog files, individual vibrational states were treated as unique molecular components. In the case where both databases contained information for a given molecule, we used the catalog that had most recently been revised and updated according to the online documentation provided by the databases.

The partition function interpolation required for such an analysis is not trivial for many molecules. In order to match the line intensities tabulated in the JPL/CDMS catalogs, we used the tabulated partition function values provided by these

databases along with the molecular catalogs. These partition function values are determined from direct summations of the Boltzmann factors of all accessible energy levels in the catalog. These values are provided in the documentation for each molecule at several specific temperature points spanning 10 to 300 K. Blake et al. (1986) showed that for either linear or nonlinear molecules, their pure rotational partition function $Q_{\rm rot}(T)$ is always proportional to T or $T^{3/2}$, respectively. Unfortunately, this pure rotational model did not always describe the tabulated partition function values provided by the databases. This was a problem in particular for molecules that possess significant internal motions, and for catalogs (and thus partition function values) merging multiple vibrational states. Therefore, we adopted the general functional form

$$Q(T) = \alpha T^{\beta}[\gamma + \exp(\epsilon/T)] \quad (1)$$

for partition function interpolation. This functional form consists of two terms: a pure $Q_{\rm rot}$ term and a $Q_{\rm rot}$ combined with a Boltzmann factor for a vibrational state. When holding part of the four coefficients to specific values, this functional form reduces to simpler cases. For example, a pure $Q_{\rm rot}$ term is derived when $\gamma = \epsilon = 0$ and $\beta = 1$ or $3/2$. For each molecule to be analyzed, we minimized the coefficients to be fitted in Equation (1), only adding additional terms if necessary to obtain a reliable fit. Since the partition function values span several orders of magnitude, the residual may not be reliable to evaluate the goodness of the interpolation. Instead, we examined the range of the relative deviation between the interpolated values and the tabulated values. This relative deviation is defined as $\delta = Q_{\rm interpolation}/Q_{\rm catalog} - 1$. For the molecules included in our analysis, this interpolation method works well in general, except for a few molecules: CH_3COCH_3, H_2CCO, H_2CO, and CH_3SH, whose maximum relative deviation exceeds 10%. We believe this level of deviation is acceptable because of the 20% uncertainty in the flux calibration in addition to the fact that the deviation is much smaller than in the other models reported (Friedel et al. 2005; Peng et al. 2013). The line catalogs, their databases and versions, the coefficients for the partition function interpolation, and the relative deviation range of our interpolation are summarized in Table 2.

The values for the source velocity, $v_{\rm lsr}$, were set to those listed in Table 1 based on information available in the literature for previous molecular observations in each source. The column density ($N_{\rm T}$), rotational temperature ($T_{\rm rot}$), line width (characterized as the FWHM), and velocity shift (δv) with respect to the source $v_{\rm lsr}$ were determined iteratively for each molecule using the procedures outlined in Rad et al. (2016). In brief, four steps were followed for each source. First, spectral lines from CO, ^{13}CO, C^{17}O, and C^{18}O were flagged in GOBASIC because of their large intensity and non-Gaussian line shapes. Data in the frequency ranges corresponding to these four lines were omitted from analysis. Second, strong spectral features arising from ubiquitous small molecules, such as CS, CN, CCH, and HCN, were fitted with arbitrary temperature and column density in GOBASIC to achieve only a best-fit model for the emission. These molecules only present a few lines in the observed frequency range, and therefore the information is not sufficient to perform a full LTE analysis. Nonetheless, their flux was properly accounted for in the analysis by using the arbitrarily fitted parameters. After that, each target molecule was analyzed using GOBASIC with the inclusion of the results from the second step. All fits were constrained within a reasonable parameter space for the search grid, where the temperature, column density, velocity shift, and line widths were held to a range of physically meaningful values; this shortened the analysis time by limiting the size of the search grid. In this initial fitting step, we determined which molecules were unambiguously detected in a source, and obtained a coarse estimate of their LTE parameters. In the final step, all detected target molecules were optimized simultaneously in GOBASIC, using their LTE parameters obtained from the third step as the initial guess for the final analysis. The convergence requirements for the change of rms of the residual and the change of parameter vector were both set to $<10^{-6}$ in GOBASIC. Caution was taken to make sure the final results did not hit the boundaries of the searching parameter space, with the exception of those cases that are specified below. Spectral lines with >1 MHz uncertainty in the catalog were discarded in our analysis to avoid unreliable assignments. Not all sources listed in Table 1 have interferometric data available in the 1.3 mm band. As a consequence, for consistency, beam dilution effects were not accounted for in our analysis, despite the ability of GOBASIC to do so. Uncertainties in the final parameters were determined from the quality of the fit as described by Rad et al. (2016), using 10^{-3} as the grid size for its numerical gradient calculation.

4. Results

The baseline-subtracted, deconvolved spectra for the 30 star-forming regions are shown in Figure 1. The spectra are plotted with intensity in units of antenna temperature, and sorted from high flux on the top to low flux on the bottom. The spectral coverage is 220–267 GHz in general, with individual variations up to 10 GHz depending on the specific spectral coverage obtained for that source. The Orion-KL survey is particularly short relative to the others, because it was used only as a benchmark to test receiver operation and deconvolution reliability. Given the extensive literature related to Orion-KL, no new astrochemical information was expected to be gained from its analysis. Likewise, although Sgr B2(N) is included here, a full analysis was not performed, because it has been so extensively studied by other groups (see Mehringer et al. 1997; Miao & Snyder 1997; Nummelin et al. 1998a, 2000; Hollis et al. 2000, 2006; Martín-Pintado et al. 2001; Remijan et al. 2002; Snyder et al. 2002; Friedel et al. 2004; Apponi et al. 2006; Halfen et al. 2006, 2011, 2013; Leigh et al. 2007; Belloche et al. 2008, 2009, 2013; Neill et al. 2014).

The CO isotopologue lines, including CO at 230.5 GHz, ^{13}CO at 220.4 GHz, C^{17}O at 224.7 GHz, and C^{18}O at 219.6 GHz, are observed in all sources. Other strong spectral features that appear in most sources include the H_2CO $3_{1,2} \rightarrow 2_{1,1}$ line at 225.7 GHz, the CN $N = 2 \rightarrow 1$ hyperfine lines at 226 GHz, the CH_3CN $J = 13 \rightarrow 12$ Q-branch at 239 GHz, the CS $J = 5 \rightarrow 4$ line at 244.9 GHz, the CH_3OH $J = 5 \rightarrow 4$ Q-branch around 242 GHz and $K_a = 3 \rightarrow 2$ R-branch around 252 GHz, the CCH $N = 3 \rightarrow 2$ hyperfine lines at 262.1 GHz, and the HCN $J = 3 \rightarrow 2$ line at 265.9 GHz. Because of the source-to-source variation of the spectral coverage, molecules such as HCN and HCO^+ are undetected in some sources simply because their lines are outside of the observed spectral window. This non-detection

Table 2
Summary of the Information of Line Catalogs

Molecule	Formula	Database	Version	Partition Function Interpolation				
				α	β	γ	ϵ	$\delta(\%)$[a]
Acetaldehyde	CH_3CHO	JPL	2012 Jan	17.1065	1.5	0.5489	−256.2868	[−0.51 0.27]
Acetone	CH_3COCH_3	JPL	2008 Mar	15274.522	1.5	0.0165	−527.2334	[−12.48 27.87]
Carbon Monosulfide	CS	CDMS	2008 Oct	0.8510	1	0	0.3957	[−0.10 0.06]
Carbon Monosulfide	^{13}CS	CDMS	2004 Jan	1.8034	1	0	0.3631	[−0.07 0.04]
Carbon Monosulfide	$^{13}C^{34}S$	CDMS	2004 Jan	0.9171	1	0	0.3593	[−0.04 0.03]
Carbon Monosulfide	$C^{33}S$	CDMS	2004 Jan	3.4325	1	0	0.3845	[−0.04 0.03]
Carbon Monosulfide	$C^{34}S$	CDMS	2004 Jan	0.8650	1	0	0.3790	[−0.07 0.04]
Carbon Monoxide Ion	CO^+	CDMS	2013 Aug	0.7105	1	0	0.9603	[−4.04 0.63]
Carbonyl Sulfide	OCS	CDMS	2005 Nov	3.4361	1	0	0	[−0.75 0.21]
Carbonyl Sulfide	$OC^{34}S$	CDMS	2005 Apr	3.5220	1	0	0	[−0.73 0.21]
Cyanide Radical	CN ($^2\Sigma^+$)	CDMS	2005 May	2.2040	1	0	0.9449	[−0.26 0.33]
Cyclopropenylidene	c-HCCCH	CDMS	2012 May	2.4549	1.5	0	0.2384	[−0.48 0.30]
Diazenylium	N_2D^+	CDMS	2009 Mar	4.9476	1	0	0	[−4.80 1.51]
Dimethyl Ether	CH_3OCH_3	CDMS	2011 Nov	91.2742	1.5	0	0	[−1.80 4.00]
Ethanol	C_2H_5OH	JPL	2008 Apr	6.6674	1.5	0.4972	−59.8213	[−0.11 0.17]
Ethenone (Ketene)	H_2CCO	CDMS	2003 Nov	1.0186	1.5	1	−3.8746	[−8.45 11.59]
Ethyl Cyanide	C_2H_5CN	JPL	2009 Jul	7.1989	1.5	0	0	[−0.38 0.17]
Ethynyl	CCH	CDMS	2010 Jul	1.9078	1	0	0.7175	[−0.13 0.16]
Formaldehyde	H_2CO	CDMS	2005 Aug	0.2791	1.5	1	−2.1456	[−9.43 14.90]
Formaldehyde	HDCO	CDMS	2000 Feb	0.3694	1.5	0	0.7692	[−2.54 3.62]
Formaldehyde	$H_2^{13}CO$	JPL	2005 Oct	0.2903	1.5	1	−2.7718	[−4.11 2.85]
Formamide	NH_2CHO	CDMS	2003 Apr	1.8945	1.5	0	0	[−4.55 1.15]
Formic Acid	*trans*-HCOOH	CDMS	2003 Jul	1.7189	1.5	0	0	[−1.20 0.38]
Formyl Cation	HCO^+	CDMS	2007 Oct	0.4671	1	0	0.7344	[−0.14 0.17]
Formyl Cation	$HC^{18}O^+$	JPL	1983 Dec	0.4894	1	0	0.6847	[−0.01 0.02]
Formyl Cation	$H^{13}CO_+$	CDMS	2007 Oct	0.4802	1	0	0.7143	[−0.12 0.15]
Formyl Radical	HCO	JPL	1983 Aug	0.5697	1.5	0	1.8171	[−2.27 4.02]
Hydrogen Cyanide	HCN	CDMS	2007 May	1.4357	1	0	0	[−5.69 1.55]
Hydrogen Cyanide	$H^{13}CN$	CDMS	2014 Nov	1.4489	1	0	0.6870	[−0.12 0.05]
Hydrogen Cyanide	$HC^{15}N$	CDMS	2005 Aug	0.4892	1	0	0	[−2.64 0.78]
Hydrogen Isocyanide	$HN^{13}C$	JPL	1979 Dec	0.4889	1	0	0	[−5.20 1.95]
Hydrogen Sulfide	H_2S	CDMS	2008 Oct	0.1015	1.5	0	0	[−5.25 2.55]
Hydrogen Sulfide	HDS	CDMS	2008 Oct	0.0797	1.5	0	2.7203	[−6.86 8.96]
Isocyanic Acid	HNCO	CDMS	2009 May	0.4451	1.5242	0	2.8006	[−7.77 5.17]
Isocyanide	DNC	CDMS	2009 Sep	0.5460	1	0	0.6251	[−0.09 0.11]
Methanethiol	CH_3SH	CDMS	2012 Jan	46.0687	1.7072	0.1085	−1244.7174	[−16.44 29.21]
Methanol	CH_3OH	JPL	2010 Mar	1.8680	1.7336	0.2229	−1005.6869	[−3.17 3.14]
Methanol	CH_2DOH	JPL	2012 Jun	0.5941	1.7821	0	0	[−4.97 5.51]
Methanol	$^{13}CH_3OH$	CDMS	2002 Dec	1.2810	1.7314	0.3372	−929.5959	[−3.12 3.13]
Methenamine	CH_2NH	JPL	1981 Jan	1.1497	1.5	0	0	[−3.52 1.19]
Methyl Cyanide	CH_3CN	CDMS	2016 Nov	1.9286	1.5	0	1.2952	[−1.94 2.11]
Methyl Cyanide	CH_3CN ($v_8 = 1$)	CDMS	2016 Nov	0.1464	2.1176	0	−481.7178	[−10.57 5.61]
Methyl Cyanide	$CH_3^{13}CN$	CDMS	2009 Dec	1.9251	1.5	0	1.2743	[−1.28 1.79]
Methyl Cyanide	$^{13}CH_3CN$	CDMS	2009 Dec	2.0506	1.5	0	0	[−10.77 2.30]
Methyl Formate	$HCOOCH_3$	JPL	2009 Apr	25.2869	1.5	0.9900	−190.5726	[−0.30 0.22]
Methylamine	CH_3NH_2	JPL	2009 Jan	23.9534	1.5	0	0	[−0.20 0.23]
Nitric Oxide	NO	JPL	2010 Oct	0.9345	1.2435	0	6.2186	[−4.16 3.89]
Nitrogen Sulfide	NS	JPL	1995 Feb	2.6639	1.1673	0	3.1202	[−4.17 4.36]
Nitrogen Sulfide	$N^{34}S$	CDMS	2011 Aug	3.9120	1.0988	0	1.6296	[−6.92 8.19]
Propyne	CH_3CCH	CDMS	2008 Aug	1.0301	1.5	1	2.4731	[−1.02 1.57]
Propyne	CH_3CCD	CDMS	2002 Apr	1.1330	1.5	1	2.4383	[−1.02 1.57]
Propyne	CH_2DCCH	CDMS	2002 Apr	1.8964	1.5	0	0	[−0.91 0.29]
Propynenitrile	HCCCN	CDMS	2000 Oct	4.6073	1	0	0	[−2.07 0.53]
Propynenitrile	HCCCN ($v_7 = 1$)	CDMS	2000 Oct	9.1357	1	0	−321.0257	[−0.01 0.00]
Propynenitrile	$H^{13}CCCN$	JPL	1979 Dec	14.2113	1	0	0	[−0.53 0.20]
Propynenitrile	$HC^{13}CCN$	JPL	1979 Dec	13.8318	1	0	0	[−0.54 0.21]
Propynenitrile	$HCC^{13}CN$	JPL	1979 Dec	13.8295	1	0	0	[−0.56 0.21]
Silicon Monoxide	SiO	JPL	1984 Jan	0.9693	1	0	0	[−2.69 1.25]
Sulfur Dioxide	SO_2	CDMS	2005 Jul	1.1492	1.5	0	0	[−3.94 1.01]
Sulfur Dioxide	$^{33}SO_2$	JPL	1996 Nov	4.6045	1.5	0	0	[−0.95 0.30]
Sulfur Dioxide	$^{34}SO_2$	JPL	1996 Nov	1.1608	1.5	0	0	[−0.95 0.30]
Sulfur Monoxide	SO	CDMS	1998 Aug	1.4598	1	1	−16.7494	[−1.19 1.95]

Table 2
(Continued)

Molecule	Formula	Database	Version	Partition Function Interpolation				
				α	β	γ	ϵ	$\delta(\%)$[a]
Sulfur Monoxide	^{33}SO	CDMS	1998 Aug	5.8908	1	1	−16.7632	[−0.89 2.16]
Sulfur Monoxide	^{34}SO	CDMS	1998 Aug	1.4851	1	1	−16.7767	[−0.83 2.36]
Sulfur Monoxide Ion	SO^+	JPL	1996 Dec	1.9142	1	0	0.0914	[−8.00 5.28]
Thioformaldehyde	H_2CS	CDMS	2008 Feb	0.5848	1.5	1	−3.2965	[−9.84 13.46]
Thioformaldehyde	HDCS	CDMS	2004 May	0.7709	1.5	0	0	[−1.73 0.55]
Thioformaldehyde	$H_2C^{34}S$	CDMS	2006 Feb	0.6004	1.5	1	−3.6703	[−4.28 3.12]
Thiomethylium	HC^{S+}	CDMS	2003 Jun	0.9871	1	0	0	[−2.55 0.90]
Vinyl Cyanide	C_2H_3CN	JPL	2009 Oct	29.1521	1.5	0.5212	−396.4232	[−0.31 0.21]
Water	HDO	JPL	1989 Oct	0.0273	1.5	0	4.7166	[−2.85 5.14]

Note. The molecules are sorted alphabetically by their chemical names. The coefficients for the interpolated partition function (Equation (1)) and the range of the interpolation deviation are listed.
[a] Deviation between the interpolated $Q(T)$ values and the catalog tabulated Q values. Listed as a range of $[\delta_{min}, \delta_{max}]$ in units of percent.

due to the limited spectral range is distinguished from the non-detection due to weak spectral intensity, which impacts the interpretation of the chemistry in these sources.

Here, because of the vast nature of the data set, we will focus the discussion on the molecules that can be reliably fit using LTE, rather than considering all possible molecular detections in the sources. A reliable LTE analysis requires the detection of sufficient unblended molecular lines that span a wide range of upper-state energy. This criterion prohibits us from reporting the abundance and temperature information for a few important COM precursors, such as H_2CO, from our analysis. Notable detections of small molecules will be mentioned, and the full analysis results can be found in Table 3, which can be retrieved in machine-readable format. In Table 3, each detected molecule is listed with four parameters and their associated uncertainties: the column density N_T in cm^{-2}, the rotational temperature T_{rot} in K, the FWHM in km s^{-1}, and the velocity shift with respect to v_{lsr}, δv, in km s^{-1}. For the molecules with insufficient information for LTE analysis, arbitrary N_T and T_{rot} may be assigned, and their associated uncertainties may be unphysical.

Figure 2 shows a sample frequency window, in which the molecular components fitted in the global LTE analysis are plotted.

Due to the complexity of the physical environment in most of these sources, molecules have a wide range of rotational temperatures and FWHMs. This is to be expected given that many of these sources have been shown through interferometric studies to have multiple kinematic components (Minh et al. 2010; Furuya et al. 2011; Friedel & Widicus Weaver 2012). Therefore, no upper-limit calculations were performed on undetected molecules. Instead, we simply report a non-detection. It is important to mention that these non-detections can be interpreted in two ways. The insufficient spectral line intensity could come from a low abundance (or non-presence) of the carrier molecule in that source, or from beam dilution if the carrier molecule's spatial distribution is compact compared to the single-dish beam.

These results can be compared to those previously reported, listed below for each source included in our data set. Due to the large number of sources, we do not provide here a comprehensive literature review of all previous observations as this is not within the scope of this manuscript. Instead, we focus on the molecules included in our analysis, especially COMs. We also do not attempt a quantitative comparison to previous results from the literature. Many of the previous observations were conducted in other wavelength ranges and therefore probed other temperature regimes and hence spatial scales. Likewise, previous observations used telescopes with different beam sizes, and there is little or no spatial scale information available for most of these sources to enable a proper beam dilution correction. Therefore, a direct, quantitative comparison is impossible. Nonetheless, we can look at overall trends in the molecules detected as well as their abundances and temperatures and draw conclusions from these results. An overview of the pertinent literature for each source and a comparison to our results are included below.

4.1. B1-b

B1-b is a dark molecular cloud with an embedded prestellar core; we observed this source at the "core" position as designated by Öberg et al. (2010). A cold complex chemistry was discovered in B1-b via the detections of CH_3OH, $HCOOCH_3$, CH_3CHO, *trans*-HCOOH, C_4H, HNCO, and the H_2C_3O isomers (Sakai et al. 2009a; Öberg et al. 2010; López-Sepulcre et al. 2015; Cuadrado et al. 2016; Loison et al. 2016), and tentatively CH_3OCH_3 (Öberg et al. 2010), as well as CH_3O (Cernicharo et al. 2012). These previous detections were all reported at levels well below the noise level obtained in our observations. Therefore, in our survey, CH_3OH was the only COM detected. Several other diatomic and triatomic molecules were detected here, including CN, CS, and HCN. The H_2CO $3_{1,2} \rightarrow 2_{1,1}$ line was also detected. Dark molecular clouds are known to have deuterium enrichment (Bergin & Tafalla 2007). We detected N_2D^+, DNC, and HDCO in B1-b, but not HDO. Other commonly detected deuterated molecules, such as DCN, DCO^+, and H_2D^+, do not have spectral lines within the spectral coverage of our survey.

4.2. GCM+0.693-0.027

GCM+0.693-0.027, located in the Sgr B2 complex, is a shocked region where COMs such as CH_3OH, C_2H_5OH, CH_3OCH_3, $HCOOCH_3$, and *trans*-HCOOH have previously been detected (Requena-Torres et al. 2006). The line shape is non-Gaussian and asymmetric, with strong absorption features at the higher frequency edge of the lines. GOBASIC can only treat Gaussian line shapes; therefore, the fit did not perfectly describe the source. Nevertheless, we could fit CH_3OH,

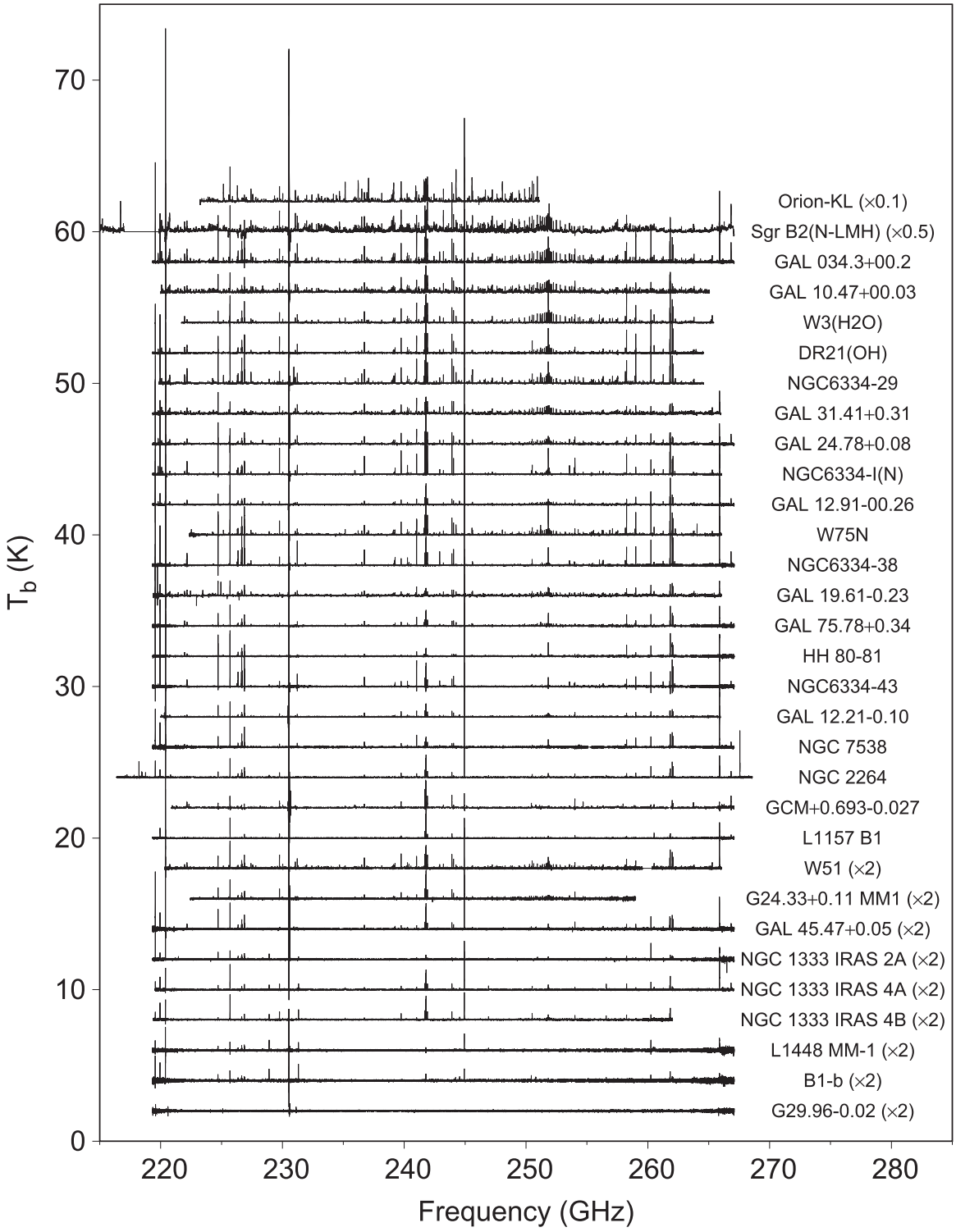

Figure 1. Baseline-subtracted, deconvolved spectra for the 30 observed sources. Spectral baselines are offset on the T_b scale for clarity. The data used to create this figure are available.

CH_3CCH, CH_2NH, H_2CS, and OCS with some confidence. The temperatures of these molecules range from 15 to 63 K. The spectral lines are extremely wide, with FWHMs from 18 to 24 km s^{-1}. The velocities are also not consistent. OCS has a blueshift of 0.6 km s^{-1}, whereas all of the other molecules display redshifts. CH_3OH and CH_3CCH are redshifted by 4 km s^{-1}, followed by H_2CS at 3 km s^{-1}, and then CH_2NH at 2 km s^{-1}. The H_2CO $3_{1,2} \rightarrow 2_{1,1}$ line was detected and fit with one Gaussian profile.

4.3. HH 80–81

HH 80–81 is a massive bipolar outflow where CH_3OH, CH_3CN, H_2CO, SO_2, SO, HCO^+, and NH_3 were observed

Table 3
Detected Molecules in the 30 Sources and Their LTE Parameters and Associated 1σ Uncertainties

Source	Molecule	N_T (cm^{-2})	T_{rot} (K)	FWHM (km s^{-1})	δv (km s^{-1})
B1-b	CH_3OH	$50 \pm 9 \times 10^{12}$	12.1 ± 1.6	1.43 ± 0.09	6.50 ± 0.05
B1-b	SO	$46 \pm 7 \times 10^{12}$	9.9 ± 0.5	1.16 ± 0.04	6.66 ± 0.02
DR21(OH)	CH_3CCH	$124 \pm 4 \times 10^{13}$	36.8 ± 1.0	5.0 ± 0.2	0.12 ± 0.07
DR21(OH)	CH_3CHO	$8 \pm 1 \times 10^{13}$	139 ± 24	5.5 ± 0.4	0.2 ± 0.1
DR21(OH)	CH_3CN	$231 \pm 5 \times 10^{11}$	56.7 ± 2.1	5.4 ± 0.2	0.63 ± 0.09
DR21(OH)	CH_3OH	$176 \pm 2 \times 10^{13}$	18.2 ± 0.3	5.63 ± 0.09	0.34 ± 0.02
DR21(OH)	CH_3OH	$152 \pm 3 \times 10^{13}$	92.8 ± 2.4	5.9 ± 0.2	0.78 ± 0.04
DR21(OH)	CH_3OCH_3	$35 \pm 2 \times 10^{13}$	60.0 ± 4.9	4.1 ± 0.4	0.3 ± 0.2
DR21(OH)	H_2CCO	$30 \pm 3 \times 10^{12}$	58.0 ± 9.7	4.8 ± 0.8	0.4 ± 0.2
DR21(OH)	H_2CS	$148 \pm 2 \times 10^{12}$	53.7 ± 1.6	5.59 ± 0.09	0.56 ± 0.04
DR21(OH)	HCCCN	$10 \pm 2 \times 10^{12}$	79 ± 12	6.0 ± 0.3	0.4 ± 0.1
DR21(OH)	$HCOOCH_3$	$107 \pm 7 \times 10^{12}$	81 ± 26	4.1 ± 0.4	0.2 ± 0.2
DR21(OH)	HDCO	$12 \pm 6 \times 10^{12}$	79 ± 42	4.8 ± 0.6	0.6 ± 0.2
DR21(OH)	OCS	$4 \pm 1 \times 10^{14}$	42.3 ± 8.5	5.4 ± 0.4	0.6 ± 0.1
DR21(OH)	SO	$431 \pm 2 \times 10^{12}$	36.2 ± 0.5	6.5 ± 0.0	0.92 ± 0.01
DR21(OH)	SO_2	$288 \pm 7 \times 10^{12}$	75.6 ± 2.6	7.7 ± 0.2	1.55 ± 0.06
DR21(OH)	^{33}SO[a]	*N/A*	*N/A*	$5.8 \pm$ *N/A*	$1.9 \pm$ *N/A*
DR21(OH)	^{34}SO[a]	*N/A*	*N/A*	$6.3 \pm$ *N/A*	$1.4 \pm$ *N/A*

Note. The four LTE parameters are the column density N_T in cm^{-2}, the rotational temperature T_{rot} in K, the FWHM in km s^{-1}, and the velocity shift with respect to v_{lsr}, δv, in km s^{-1}. 1σ uncertainties are reported. Only molecules with more than three unblended lines at different upper-state energies can be fitted to a reliable T_{rot}. Other small molecules are fitted with arbitrary N_T and T_{rot}, and their associated uncertainties may be unphysically large.
[a] Spectral lines of this molecule are detected, but they are insufficient to perform a reliable LTE analysis. Only the FWHM and δv are reported here, without their unphysical uncertainties. The full set of determined parameters for reproducing our best-fit spectra are given in the machine-readable table.

(This table is available in its entirety in machine-readable form.)

(Martí et al. 1993; Gómez et al. 2003; Qiu & Zhang 2009). In our survey, we reliably fit CH_3OH, CH_3CCH, H_2CS, SO, and SO_2. The molecules are cold, with the hottest one being SO_2 at 47 K. The other four molecules are within 15–25 K. The spectral lines are also narrow, with FWHMs from 1.5 to 3.1 km s^{-1}. The velocities are consistent within 1 km s^{-1}. The asymmetric H_2CO $3_{1,2} \rightarrow 2_{1,1}$ line was modeled with two Gaussian components.

4.4. L1157

The L1157 region is a bipolar outflow from the central star L1157 MM. We observed the B1 position in the outflow based on the interferometric study of Arce et al. (2008). Millimeter single-dish and interferometry studies on small molecules (CS, SiO, etc.), CH_3OH, and CH_3CN have revealed the outflow structure and molecular component (Avery & Chiao 1996; Codella et al. 2009; Flower et al. 2010; Gómez-Ruiz et al. 2013; Burkhardt et al. 2016). Additional observations were conducted in the submillimeter by the CHESS project on *Herschel* (Codella et al. 2010, 2012; Lefloch et al. 2010, 2012; Benedettini et al. 2012; Busquet et al. 2014). Bachiller & Gutiérrez (1997) and Bachiller et al. (2001) reported spectral lines from CH_3OH, H_2CO, SiO, HCN, CN, CS, SO, and SO_2 in the 1.3 mm band using the IRAM 30 m telescope. Another line survey reported the detection of $HCOOCH_3$, CH_3CN, HCOOH, and C_2H_5OH in its B1 shock region, which is in the blueshifted lobe of L1157 (Arce et al. 2008).

In our survey of the B1 region, we confirmed the detection of small molecules reported by Bachiller & Gutiérrez (1997) and Bachiller et al. (2001), except for the SO_2 lines, which were too weak to be observed. No spectral features, however, were found for any of the COMs reported by Arce et al. (2008). This is likely due to beam dilution, as the COM detections showed small spatial scales relative to the CSO beam. The spectral line shape in L1157 is asymmetric. We fit two velocity components to methanol and SO, one with a blueshift of 3.7–3.9 km s^{-1} and a wider FWHM of 6 km s^{-1}, another one with a blueshift of 1 km s^{-1} and a narrower FWHM of 3–3.6 km s^{-1}. The narrower component corresponds to the north region, where the lines are redshifted from the gas extending farther out from the star. The wider component corresponds to the south region toward the B1 and B2 blueshifted lobes. The molecules are extremely cold, with rotational temperatures below 15 K, and do not perfectly follow a Boltzmann intensity profile. Nevertheless, we can estimate the methanol column density to be 1.2×10^{15} cm^{-2}, and the SO column density to be 1.8×10^{14} cm^{-2}. The column density ratio between methanol and SO agrees well with that reported by Bachiller & Gutiérrez (1997). The asymmetric H_2CO $3_{1,2} \rightarrow 2_{1,1}$ line was modeled with two Gaussian components.

4.5. L1448 MM-1

The L1448 MM-1 source is a bipolar outflow. We observed the C(N) position. This source has been studied previously in the millimeter band (Bachiller et al. 1991; Gregersen et al. 1997; Maret et al. 2004; Jørgensen et al. 2005b, 2007; Maret et al. 2005; Requena-Torres et al. 2007). In these surveys, HCO^+, $H^{13}CO^+$, $HN^{13}C$, SiO, H_2CO, and CH_3OH were detected. Parise et al. (2006) studied the deuterated chemistry in detail using the HDCO, D_2CO, CH_2DOH, and CH_3OD lines. In the 3 mm band, the long carbon chain molecule C_4H was also observed (Sakai et al. 2009a). We confirmed the presence of CH_3OH and H_2CO lines in the 1.3 mm band. In addition to CH_3OH and H_2CO, we detected CS, CN, and HCN. We observed a high D/H ratio, indicated by strong lines from DNC, N_2D^+, and HDCO.

The spectral lines are much narrower, compared to the outflow of L1157. An FWHM of 1.5 km s^{-1} was found for CS,

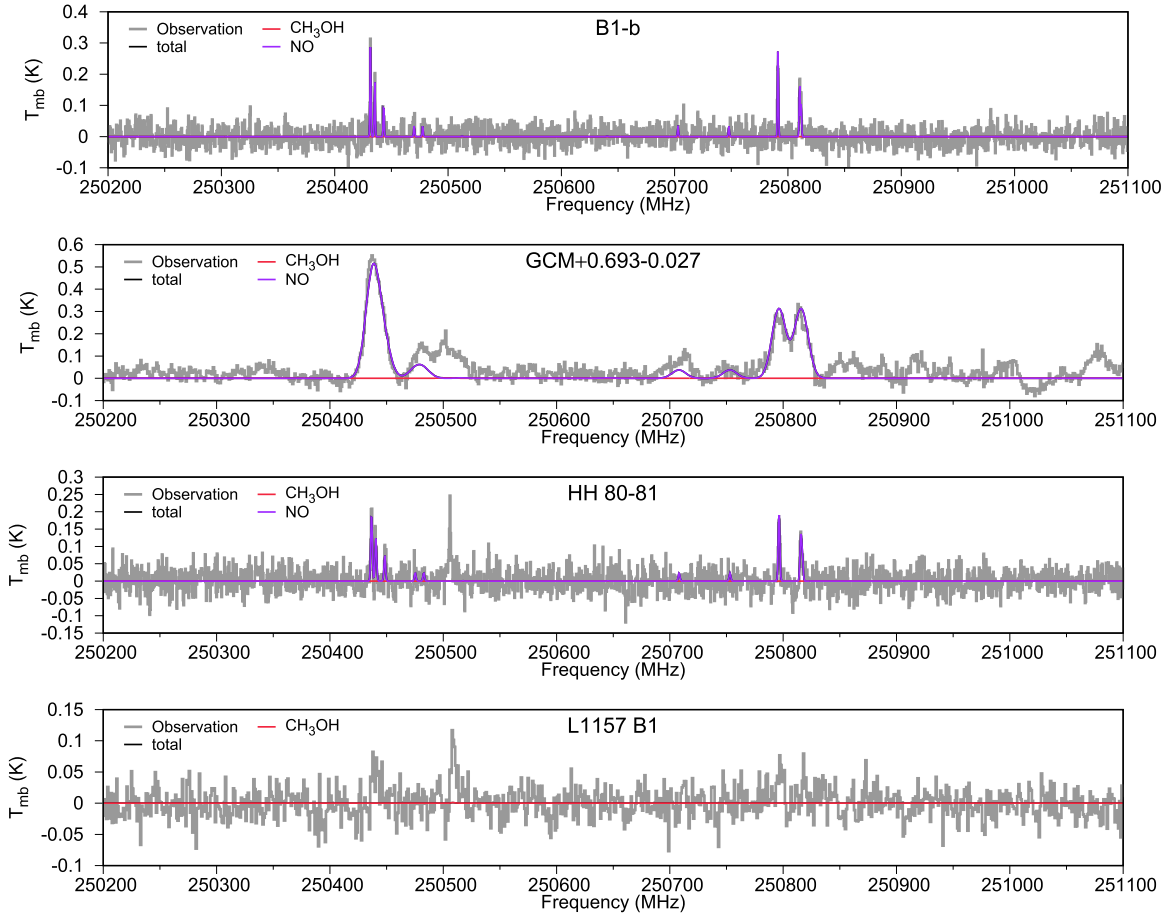

Figure 2. Sample frequency window of the molecular components fitted in the global LTE analysis. The CH_3OH line at 250510 MHz is non-LTE in some of the sources.

(The complete figure set (29 images) is available.)

and line widths were narrower for the other detected molecules. CH_3OH has a rotational temperature of 17.7 K, slightly warmer than L1157. We only observed one main velocity component, which is redshifted from the central star rest velocity by 5–6 km s^{-1}. The H_2CO $3_{1,2} \rightarrow 2_{1,1}$ line was detected and fit with one Gaussian profile.

4.6. NGC 6334

NGC 6334, also called the Cat's Paw nebula, is a H II region that contains several massive protostars (Straw et al. 1989). Although it has been studied in the infrared and millimeter for its star formation processes (e.g., Persi et al. 2000; Hunter et al. 2006; Brogan et al. 2009), only a few molecular surveys are available for this source (Bisschop et al. 2007; Thorwirth et al. 2007; Walsh et al. 2010). In these surveys, COMs such as CH_3OH, $^{13}CH_3OH$, CH_3CCH, CH_3CN, $CH_3^{13}CN$, C_2H_5OH, $HCOOCH_3$, CH_3OCH_3, NH_2CHO, C_2H_5CN, and *trans*-HCOOH were detected. CH_3OH masers in the millimeter were also reported (Slysh et al. 2002).

We pointed to four Class 0 star-forming regions, NGC 6334–29, NGC 6334–38, NGC 6334–43, and NGC 6334-I(N), in this nebula. In general, rich chemistry was found in NGC 6334–29 and NGC 6334-I(N), whereas NGC 6334–38 and NGC 6334–43 have simpler chemistry.

In NGC 6334–29, we were able to fit 17 molecules with reliable temperatures, in addition to another 25 small molecules. For O-containing molecules, we detected CH_3OH, $^{13}CH_3OH$, CH_3OCH_3, H_2CCO, $HCOOCH_3$, and CH_3CHO. For N-containing molecules, we detected CH_3CN, $^{13}CH_3CN$, HCCCN (ground state and $v_7 = 1$), NH_2CHO, CH_2NH, and C_2H_5CN. For S-containing molecules, we detected H_2CS, OCS, SO, SO_2, and $^{34}SO_2$. CH_3CCH is also abundant. CH_3OH has a cold component at 19 K and a warm component at 128 K. $HCOOCH_3$ is the warmest molecule detected, with a temperature of 285 K. The S-containing molecules in NGC 6334–29 are kinematically different from the rest of the COMs. Instead of having a Gaussian line shape with FWHMs of 4–6 km s^{-1}, S-containing molecules show broadening in their line shapes. We modeled this with a convolution of two Gaussian components, a narrow one of 4 km s^{-1}, and a wide one of 8–13.5 km s^{-1}. The two components have similar temperatures for each molecule. SO_2, however, does not show these two components. Instead, it shows a cold component at 13 K, and a warm component at 138 K, similar to CH_3OH.

NGC 6334-I(N) is in an early cluster formation stage with molecular outflows but rather weak mid-IR emission (Megeath & Tieftrunk 1999). It contains seven submillimeter continuum sources in a roughly $15'' \times 15''$ region, with an estimated total gas mass of 39–145 $M_\odot$ (Hunter et al. 2006; Brogan et al. 2009). Walsh et al. (2010) acquired a low-resolution map toward a $5' \times 5'$ region around NGC 6334-I(N) and found the peak fluxes of CH_3OH, CH_3CN, H_2CS, HCCCN, OCS, and SO

on the source site. Spectral lines were also reported by Brogan et al. (2009) in the 1.3 mm band from their SMA maps. Detected molecules included CH_3OH, $HCOOCH_3$, C_2H_3CN, CH_3OCH_3, H_2CO, and HCCCN.

In our survey of NGC 6334-I(N), we were able to fit 15 molecules with reliable temperatures, in addition to another 21 small molecules. For O-bearing molecules, we only detected CH_3OH, $^{13}CH_3OH$, CH_3OCH_3, CH_3CHO, and H_2CCO. For N-bearing molecules, we only detected CH_3CN, CH_2NH, and HCCCN. For S-bearing molecules, we only detected H_2CS, OCS, SO, and SO_2. CH_3CCH is also abundant. Interestingly, despite the rich chemistry in NGC 6334-I(N), all molecules are cold. The temperature range is only 10–35 K, a temperature range more typical for prestellar cores. The reason for NGC 6334-I(N) having such a rich COM inventory at such a low temperature is not clear; it is possible there is an outflow driving shocks. The FWHMs are in the range of 3–9 km s^{-1}. We observed an asymmetric line shape, similar to NGC 6334–29, for SO, but not for other S-bearing molecules. Instead, CH_3OH in NGC 6334-I(N) shows a similar asymmetric line shape, with a narrow component at 3.4 km s^{-1} and a wider component at 6.9 km s^{-1}. The temperature difference between these two CH_3OH components is only 4 K. The velocities range from 0.5 km s^{-1} redshift to 2.2 km s^{-1} blueshift.

In NGC 6334–38, we were able to fit nine molecules with reliable temperatures, in addition to another 26 small molecules. For O-bearing molecules, we only found CH_3OH and H_2CCO. For N-bearing molecules, we only found CH_3CN and HCCCN. For S-bearing molecules, we only found OCS and SO. CH_3CCH is also present. All molecules have temperatures within the range of 20–50 K, much colder than NGC 6334–29. The lines are 3–5 km s^{-1} wide in FWHM, with a consistent redshift of 1.5–2.6 km s^{-1} with respect to the source's v_{lsr}.

In NGC 6334–43, we were able to fit seven molecules with reliable temperatures, in addition to 18 other small molecules. For O-bearing molecules, we only found CH_3OH and H_2CCO. For N-bearing molecules, we only found CH_3CN and HCCCN. For S-bearing molecules, we only found OCS and SO. CH_3CCH is also present. All molecules have temperatures within the range of 10–35 K, even colder than NGC 6334–38. The lines are 3–4 km s^{-1} wide in FWHM, with a consistent redshift of 1.9–2.6 km s^{-1} with respect to the source v_{lsr}.

An asymmetric H_2CO $3_{1,2} \rightarrow 2_{1,1}$ line was found in all four regions in NGC 6334. In NGC 6334–29, −38, and −43, it was modeled with two Gaussian components; in NGC 6334-I(N), it was modeled with three Gaussian components.

4.7. NGC 1333

NGC 1333 is a fragmented molecular cloud with multiple low-mass protostars embedded. Intensive studies have focused on this low-mass star-forming region (Blake et al. 1995; Gregersen et al. 1997; Bachiller et al. 1998; Stark et al. 1999; Knee & Sandell 2000; Bottinelli et al. 2004, 2007; Jørgensen et al. 2004, 2005a, 2005b, 2007; Maret et al. 2004, 2005; Wakelam et al. 2005; Parise et al. 2006; Plume et al. 2007; Choi et al. 2010; Sakai et al. 2012, 2006; Coutens et al. 2013, 2015; Lyo et al. 2014; Taquet et al. 2015; De Simone et al. 2017). Numerous COMs, such as CH_3CN, CH_3OH, CH_2DOH, $^{13}CH_3OH$, *trans*-HCOOH, $HCOOCH_3$, CH_3OCH_3, C_2H_5OH, C_2H_5CN, and CH_2OCHO, were detected in the IRAS 2 and IRAS 4A regions in this cloud (Blake et al. 1995; Bachiller et al. 1998; Bottinelli et al. 2004, 2007; Jørgensen et al. 2004, 2005a, 2005b, 2007; Maret et al. 2005; Parise et al. 2006; Sakai et al. 2012; Coutens et al. 2015; Taquet et al. 2015; De Simone et al. 2017). $(CH_2OH)_2$ was also detected in IRAS 2 (Coutens et al. 2015). The IRAS 4B core has fewer COMs reported: CH_3CN, CH_3OH, CH_2DOH, CH_3OD, $HCOOCH_3$, and CH_2OHCHO (Jørgensen et al. 2005b; Maret et al. 2005; Parise et al. 2006; Sakai et al. 2006, 2012; De Simone et al.v 2017).

In our survey, we observed three positions in NGC 1333: the IRAS 2A, 4A, and 4B regions. We also conducted observations on NGC 1333 IRAS 2B, but found after the observations were complete that the incorrect source position was used. Our survey revealed a relatively simple chemical composition of these sources, which is not surprising given that the COMs previously detected in these sources using single-dish observations were detected at signal intensities of $\leqslant$10 mK, which is our noise level (see Bottinelli et al. 2007 for an example). In the three regions observed, only CO, CS, cold CH_3OH, and the H_2CO $3_{1,2} \rightarrow 2_{1,1}$ line were detected. We could only reliably fit the cold CH_3OH, which is 15–25 K, and has a non-Gaussian, asymmetric line shape. The total spectral flux of 4A and 4B is higher than that of 2A. In 4A and 4B, it is likely that they contain a warmer CH_3OH component, indicated by weak spectral features around the warm CH_3OH $K_a = 3 \rightarrow 2$ R-branch near 252 GHz. However, the signal-to-noise ratio is too low to generate a reliable LTE fit. In addition, two CH_3OH lines, $8_{-1,8} \rightarrow 7_{0,7}$($E_{low}$ = 78 K) at 229.76 GHz, and $11_{0,11} \rightarrow 10_{1,10}$($E_{low}$ = 141 K) at 250.51 GHz, present inconsistently high intensities which indicates the non-LTE environment of these sources. The H_2CO $3_{1,2} \rightarrow 2_{1,1}$ line was modeled with a single Gaussian in 2A, whereas 4A and 4B were modeled using two Gaussian components.

The weak intensity of COM lines in NCG 1333 sources is likely due to their small source sizes, which result in a heavy beam dilution effect. The warmer lines from other COMs are likely below the noise level. To study these hot corinos, telescopes with smaller beam size and higher spatial resolution are required.

4.8. GAL 75.78+0.34

GAL 75.58+0.34 is a massive star-forming region and a hypercompact H II region (Kurtz 2005; Bisschop et al. 2007; Riffel & Lüdke 2010). CH_3OH, $^{13}CH_3OH$, CH_3CN, CH_3CCH, and SO_2 were detected in a 1.3 and 0.89 mm line survey (Hatchell et al. 1998b). CH_3OH and CH_3CN lines were also studied by Pankonin et al. (2001) and Sánchez-Monge et al. (2013). Bisschop et al. (2007) detected H_2CO, CH_3OH, $^{13}CH_3OH$, H_2CCO, CH_3OCH_3, $HCOOCH_3$, *trans*-HCOOH, CH_3CCH, CH_3CN, and NH_2CHO in this source with temperatures between 40 and 190 K. We reliably fit CH_3OH, CH_3CCH, CH_3CN, H_2CCO, H_2CS, HCCCN, OCS, SO, and SO_2. CH_3OH has a cold component at 15 K and a warm component at 160 K, and is the hottest molecule in this source. Other than the warm CH_3OH, the remaining molecules are below 100 K. Comparing GAL 75.78+0.34 and GAL 45.47 +0.05, the former seems to be at a later stage in the star formation process, because of the presence of warm CH_3OH and CH_3CN (92 K). The FWHMs are 3–6 km s^{-1}, and the velocities are between −4 and −3 km s^{-1}. The asymmetric

H_2CO $3_{1,2} \rightarrow 2_{1,1}$ line was modeled with two Gaussian components.

4.9. GAL 12.21–0.10

GAL 12.21–0.10 is a hot core embedded in an ultracompact H II region (de la Fuente et al. 2010). A few line surveys in the 1.3 and 0.89 mm bands have been reported toward this source, where several COMs were detected (Hatchell et al. 1998a, 1998b; Pankonin et al. 2001). These COMs include CH_3OH and its isotopologue $^{13}CH_3OH$, CH_3CN, and CH_3CCH. Here, we present the detection of a handful of COMs at moderate temperatures, supporting the existence of a hot core. We reliably fit CH_3OH, CH_3OCH_3, CH_3CCH, CH_3CN, H_2CCO, H_2CS, HCCCN, OCS, SO, and SO_2. CH_3OH has two temperatures, a cold component at 16 K and a warm component at 162 K. For other molecules, instead of clustering into cold and warm groups, their temperatures range widely from 20 to 150 K. CH_3OCH_3 and SO_2 are warm, whereas CH_3CCH and SO are cold. The FWHMs of these molecular lines are around 7–10 km s^{-1}, and the velocities are consistent within −1 to 1 km s^{-1}. The H_2CO $3_{1,2} \rightarrow 2_{1,1}$ line was detected and fit with one Gaussian profile.

4.10. NGC 2264

NGC 2264 is a star-forming region with multiple millimeter continuum sources (Ward-Thompson et al. 2000). We pointed at the NGC 2264 C-MM3 source, where the peak CH_3OH intensity is located (Sakai et al. 2007; Saruwatari et al. 2011), and a rich chemistry was observed by combining extensive Nobeyama 45 m dish (4 and 3 mm) and ASTE 10 m dish (0.89 mm; Watanabe et al. 2015). CH_3OH, $^{13}CH_3OH$, CH_3CCH, HC_5N, CH_3CN, CH_3CHO, H_2CCO, CH_3OCH_3, $HCOOCH_3$, and NH_2CHO lines were detected in this survey. A 1.3 mm SMA map, however, reveals a C-MM4 core that has much higher continuum emission and more molecules than C-MM3 (Cunningham et al. 2016). C-MM4 is about 30″ away from C-MM3.

In our survey, we detected abundant CH_3OH, along with CH_3CCH, H_2CO, HDCO, H_2CS, and SO. More complex COMs, such as CH_3CHO, CH_3OCH_3, and $HCOOCH_3$, were not found. A consistent velocity component of 0–1 km s^{-1} with 4–5 km s^{-1} FWHM can be fit to the above molecules. The rotational temperature ranges from 20 to 50 K.

$HCOOCH_3$ was reported as a detection in NGC 2264 MMS3 (Sakai et al. 2007) in the 3 mm band using the Nobeyama 45 m radio telescope. The A/E lines from the $8_{1,8} \rightarrow 7_{1,7}$ transition of $HCOOCH_3$ were observed at a main beam temperature intensity of 60–80 mK. The signal-to-noise ratio of that detection was only 2–3. In our 1.3 mm band survey, no $HCOOCH_3$ was detected. The peak-to-peak noise level of our survey is ∼50 mK. Considering a CSO beam (30″) that is larger than the Nobeyama beam (19″) and a higher frequency band, which in general means lines arising from warmer gas, it is likely that the $HCOOCH_3$ lines are below our detection limit. The H_2CO $3_{1,2} \rightarrow 2_{1,1}$ line was detected and fit with one Gaussian profile.

4.11. NGC 7538

NGC 7538 is a high-mass star-forming region with massive protostars and outflows (Scoville et al. 1986; Kraus et al. 2006), the IRS 1 core being one of the protostars (Buizer & Minier 2005). H_2CO, CH_3OH, and CH_3CN were detected in the millimeter bands (Slysh et al. 1999; Kalenskii et al. 2000a, 2000b; van der Tak et al. 2000; Wirström et al. 2011), and one C_2H_5OH line was reported in the centimeter (Menten et al. 1986). Ikeda et al. (2001) detected c-C_2H_4O and CH_3CHO in this source. Bisschop et al. (2007) detected H_2CO, CH_3OH, $^{13}CH_3OH$, H_2CCO, $HCOOCH_3$, C_2H_5OH, CH_3CHO, *trans*-HCOOH, CH_3CCH, and NH_2CHO, and gave upper limits for CH_3CN, C_2H_5CN, and CH_3OCH_3. Among these molecules, the hottest ones are CH_3OH at 156 K, C_2H_5OH and NH_2CHO, both at 164 K, and $HCOOCH_3$ at 134 K. The rest of the molecules are below 100 K.

In our survey, we detected CH_3OH, H_2CCO, CH_3CCH, CH_3CN, H_2CS, HCCCN, SO, and SO_2. CH_3OH has two components, a cold one at 24 K and a warm one at 257 K. CH_3CN is the other warm molecule in this source, with a temperature of 244 K. Due to the low signal-to-noise ratio of the CH_3CN lines, its temperature is subject to a large uncertainty. Nonetheless, the value 244 K can be treated as an upper limit. The remaining molecules are between 13 and 66 K, which agrees with the result from Bisschop et al. (2007). The FWHMs are from 3 to 4.5 km s^{-1}. All of the lines are blueshifted within the range of 0–2.4 km s^{-1}. The asymmetric H_2CO $3_{1,2} \rightarrow 2_{1,1}$ line was modeled with two Gaussian components.

4.12. GAL 45.47+0.05

GAL 45.47+0.05 is an ultracompact H II region (Cesaroni et al. 1992; Hofner et al. 1999) with outflows (Ortega et al. 2012). Remijan et al. (2004a) reported the detection of CH_3CN in the 3 mm band using BIMA, and the CH_3CN was further mapped by Hernández-Hernández et al. (2014). Other COMs, such as CH_3OH, $^{13}CH_3OH$, CH_3CCH, CH_3OCH_3, C_2H_5CN, and C_2H_3CN, were reported in several millimeter-band line surveys (Hatchell et al. 1998b; Fontani et al. 2007).

In our 1.3 mm band survey, we fit six molecules with reliable temperatures: CH_3OH, CH_3CCH, H_2CS, HNCO, SO, and SO_2. Among them, only two are COMs. We did not detect CH_3CN. The gas temperatures are low with SO_2 being the hottest one at 44 K. The FWHMs are between 4 and 6 km s^{-1}. The velocity shifts with respect to v_{lsr} span between 0 and 2.3 km s^{-1}. The H_2CO $3_{1,2} \rightarrow 2_{1,1}$ line was detected and fit with one Gaussian profile.

4.13. GAL 12.91–00.26

GAL 12.91–00.26 is a massive hot core. CH_3OH, CH_3CN, CH_3OCH_3, $HCOOCH_3$, and C_2H_5CN lines were reported by several line surveys across the millimeter bands (Slysh et al. 1999; van der Tak et al. 2000; Purcell et al. 2006; Reiter et al. 2011; He et al. 2012). Its rich chemistry was reported by Bisschop et al. (2007) using IRAM and JCMT. In their study, they detected CH_3OH, $^{13}CH_3OH$, C_2H_5OH, CH_3OCH_3, $HCOOCH_3$, H_2CO, NH_2CHO, and CH_3CN at elevated temperatures. In addition to these hot COMs, they also detected H_2CCO, *trans*-HCOOH, and CH_3CCH at cold temperatures. C_2H_5CN and CH_3CHO were reported as upper limits.

In our survey, we reliably fit CH_3OH, $^{13}CH_3OH$, CH_3OCH_3, CH_3CCH, CH_3CN, CH_2NH, H_2CCO, H_2CO, HCCCN, $HCOOCH_3$, OCS, SO, and SO_2. We also detected lines from the $v_7 = 1$ vibrational excited state of HCCCN. CH_3OH has two temperature components, a cold one at 14 K and a warm

one at 178 K. Similarly, CH_3OCH_3, CH_3CN, HCCCN, and $HCOOCH_3$ are warm, with temperatures above 100 K. The rest of the molecules, especially CH_3CCH and CH_2NH, are cold. This result agrees with that of Bisschop et al. (2007). The FWHM of these molecules are about 3–6 km s^{-1}. The asymmetric H_2CO $3_{1,2} \rightarrow 2_{1,1}$ line was modeled with two Gaussian components.

4.14. GAL 19.61–0.23

GAL 19.61–0.23 is identified as a hot molecular core by multiple line surveys. In the 3 mm band, CH_3OH, CH_3CN, C_2H_5CN, HCOOCH, and *trans*-HCOOH were detected (Remijan et al. 2004a; Furuya et al. 2005). In the 2 and 1.3 mm bands, C_2H_5CN, C_2H_3CN, CH_3OCH_3, CH_3CN, $HCOOCH_3$, CH_2NH and CH_2OHCHO (glycoaldehyde) were reported (Fontani et al. 2007; Calcutt et al. 2014; Favre et al. 2014; Suzuki et al. 2016). Wu et al. (2009) and Furuya et al. (2011) mapped the CH_3CN emission in the 890 μm band. Qin et al. (2010) compiled a list of molecules detected from a line survey in a 2 GHz window in the SMA 890 μm band. CH_3OH, $^{13}CH_3OH$, CH_3OCH_3, $HCOOCH_3$, C_2H_5OH, $CO(CH_2OH)_2$, NH_2CHO, and CH_3CN were reported with multiple unblended spectral lines observed. CH_3CHO, CH_2NH, $^{13}CN_3CN$, $CH_3^{13}CN$, C_2H_5CN, and *trans*-HCOOH were reported with either only one detected spectral line, or with multiple lines that are blended with other molecular lines.

Our 1.3 mm broadband line survey supports the rich chemistry discovered by previous line surveys. We reliably fit CH_3OH, $^{13}CH_3OH$, CH_3OCH_3, CH_3CCH, CH_3CN, C_2H_3CN, C_2H_5CN, H_2CCO, H_2CS, HCCCN, $HCOOCH_3$, HNCO, OCS, SO, and SO_2. However, we did not find a reliable detection of CH_3CHO, CH_2NH, $^{13}CN_3CN$, $CH_3^{13}CN$, C_2H_5OH, and NH_2CHO. $CO(CH_2OH)_2$ was not included in the list of molecules that were analyzed in this source. CH_3OH has two components, a cold one at 14 K and a warm one at 177 K. This result is different from Qin et al. (2010), who fit a single temperature of 151 K in their Boltzmann diagram despite the fact that a cold CH_3OH line has a significantly higher $\ln(N_u)/g_u$ value than the rest of the warm CH_3OH lines. For most of the other detected molecules, our analysis shows a lower rotational temperature with smaller uncertainties. This is because the global analysis of GOBASIC is less likely to overpredict the spectral intensity from a single molecule in a blended line. Still, the trend is similar to that shown by Qin et al. (2010). N-bearing molecules, including CH_3CN, C_2H_5CN, and HNCO, are found to be at higher temperatures. The FWHM of these lines spans a wide range, from 4 to 14 km s^{-1}. COMs are generally found to have FWHMs of 7–9 km s^{-1}, with the exception of $^{13}CH_3OH$, which is 4.6 km s^{-1}. The asymmetric H_2CO $3_{1,2} \rightarrow 2_{1,1}$ line was modeled with two Gaussian components.

4.15. G24.33+00.11 MM1

G24.33+0.14 is listed as an outflow candidate in the Extended Green Objects catalog (Cyganowski et al. 2008). It is a high-mass young stellar object that has not yet formed a compact H II region. This stellar core was mapped in the 890 μm band by the SMA using molecular lines from CH_3CN, $^{13}CH_3CN$, CH_3OH, CH_3OCH_3, SO, and ^{34}SO, and a few other COMs such as C_2H_5OH and NH_2CHO were tentatively detected (Rathborne et al. 2011). We pointed to the stellar core G24.33+00.11 MM1 at $\alpha = 18^h35^m08^s.14$, $\delta = -07°35'01''.1$, which is offset from the nominal source position of $\alpha = 18^h35^m08^s.1$, $\delta = -07°35'04''$. The flux of G24.33 +00.11 MM1 is weaker compared to that of other hot cores we observed. Nevertheless, it is one of the sources displaying the richest chemistry. In addition to the commonly detected CH_3OH, CH_3OCH_3, CH_3CCH, CH_3CN, H_2CCO, H_2CS, HCCCN, $HCOOCH_3$, OCS, and SO, we reliably fit C_2H_5CN, C_2H_5OH, CH_2NH, $^{13}CH_3OH$, and CH_3CN ($v_8 = 1$). Interestingly, we did not detect SO_2. The hottest molecules are CH_3CN (302 K), warm CH_3OH (233 K), CH_3OCH_3 (200 K), and $HCOOCH_3$ (124 K). CH_3OH also has a cold component at 14 K. Because we treated vibrational states as individual molecules, the CH_3CN ($v_8 = 1$) temperature is 150 K, lower than the vibrational ground state. The rest of the COMs are below 100 K. The FWHMs of the lines are 3–5 km s^{-1}. The asymmetric H_2CO $3_{1,2} \rightarrow 2_{1,1}$ line was modeled with two Gaussian components.

4.16. GAL 24.78+0.08

GAL 24.78+0.08 is an embedded cluster with high-mass protostars (Furuya et al. 2002). It possesses a rotation toroid (Beltrán et al. 2005) and gas infall accompanied by outflows (Cesaroni et al. 2003; Beltrán et al. 2006, 2011). In these observations, CH_3OH, H_2CCO, CH_3OCH_3, C_2H_5CN, C_2H_3CN, C_2H_5OH, and $HCOOCH_3$ lines were reported, and CH_3CN and $CH_3^{13}CN$ were used as kinematic tracers. Molecular lines from CH_3OH, CH_3OD, CH_3CN, $HCOOCH_3$, and C_2H_5CN were also reported in other surveys in the centimeter and millimeter bands (Purcell et al. 2006; Vig et al. 2008; Ratajczak et al. 2011; Calcutt et al. 2014; Favre et al. 2014). Bisschop et al. (2007) reported the detection of H_2CO, CH_3OH, C_2H_5OH, NH_2CHO, CH_3CN, C_2H_5CN, $HCOOCH_3$, CH_3OCH_3, H_2CCO, CH_3CCH, and *trans*-HCOOH. The rotational temperature of these molecules ranges from 39 to 261 K. Specifically, glycolaldehyde (CH_2OHCHO) was reported as a detection in this source (Beltrán et al. 2005; Calcutt et al. 2014).

In our analysis, we reliably fit CH_3OH, $^{13}CH_3OH$, CH_3OCH_3, CH_2NH, CH_3CCH, CH_3CN, H_2CS, HCCCN, $HCOOCH_3$, OCS, SO, and SO_2. CH_3OH has a cold component at 17 K and a warm component at 141 K. We also detected the HCCCN $v_7 = 1$ vibrational excited state. The temperatures of CH_3OH, CH_3OCH_3, $HCOOCH_3$, HCCCN ($v_7 = 1$), and CH_3CN are above 100 K. CH_3CN is the hottest molecule, with a temperature of 204 K. This temperature of CH_3CN is slightly lower than the 261 K reported by Bisschop et al. (2007), but higher than the 132 K reported by Beltrán et al. (2005), who combined the lines from the normal species, the ^{13}C isotopologue, and the $v_8 = 1$ vibrational state in their analysis. The FWHMs of the lines are 5–9 km s^{-1}. The asymmetric H_2CO $3_{1,2} \rightarrow 2_{1,1}$ line was modeled with two Gaussian components.

4.17. DR21(OH)

DR21(OH), located in the Cygnus X complex, is a giant, fragmented molecular cloud with multiple emission cores (Minh et al. 2012; Girart et al. 2013). Small molecules such as CS, OCS, H_2CO, HDCO, H_2CS, and c-C_3H_2 (cyclopropenylidene) have been observed in the centimeter band toward this cloud (Angerhofer et al. 1978; Goldsmith & Linke 1981;

Madden et al. 1989; Chandler et al. 1993; Richardson et al. 1994; Mehringer et al. 1995; Wootten & Mangum 2009). Numerous COMs, such as CH_3OH, CH_3CN, CH_3CHO, c-C_2H_4O, CH_3CCH, CH_3OCH_3, C_2H_5CN, and CH_2NH, were detected in multiple line surveys in the 3, 2, 1.3, and 0.89 mm bands (Kalenskii et al. 1997, 2000a, 2000b; Slysh et al. 1999, 2002; van der Tak et al. 2000; Ikeda et al. 2001; Alakoz et al. 2002; Charnley 2004; Kalenskii & Johansson 2010a; Wirström et al. 2011; Zapata et al. 2012; Girart et al. 2013; Suzuki et al. 2016). Kalenskii & Johansson (2010a) found low to moderate rotational temperatures, 9–56 K, for most molecules detected. The evidence for the existence of an embedded hot core is the hot rotational temperature of CH_3OH at 252 K and SO_2 at 186 K.

Our results agree well with those of Kalenskii & Johansson (2010a) and Minh et al. (2012) in the type of molecules detected. In brief, two methanol temperature components were observed, indicated by the coexistence of the cold methanol branch at 242 GHz and the warm methanol branch between 250 and 253 GHz. The temperature of the warm methanol, however, is 93 K and significantly lower than the value reported by Kalenskii & Johansson (2010a). It is possible that heavy beam dilution diminished the weaker lines of the methanol branch into the noise, which led to our lower estimation of the rotational temperature. Other detected COMs include CH_3CN, CH_3CCH, CH_3CHO, CH_3OCH_3, H_2CCO, HCCCN, and $HCOOCH_3$. No rigorous detections of *trans*-HCOOH, NH_2CHO, and C_2H_3CN were found, despite being reported by Kalenskii & Johansson (2010a). The two tentative detections reported by Kalenskii & Johansson (2010a), CH_2NH and C_2H_5OH, were also not found. The LTE temperatures of the COMs we detected are all below 150 K, with CH_3CHO being the warmest one at 139 K. The FWHMs of these molecular lines are consistent within the range of 4–7 km s^{-1}. The asymmetric H_2CO $3_{1,2} \rightarrow 2_{1,1}$ line was modeled with three Gaussian components.

Multiple methanol masers have been observed in the DR21 complex (Plambeck & Menten 1990; Araya et al. 2009; Fish et al. 2011). Similarly, we also observed non-LTE methanol emission at 229.76 GHz ($8_{-1,8} \rightarrow 7_{0,7}$) and 250.5 GHz ($11_{0,11} \rightarrow 10_{1,10}$, A^+), as the total flux of these two methanol lines considerably exceeds the LTE emission at 93 K. These two lines may be associated with the same physical environment that drives the methanol masers at lower frequencies. The rest of the molecular lines can be modeled with the LTE model.

4.18. W75N

W75N is an ultracompact H II region associated with high-mass star formation (Persi et al. 2003). Watson et al. (2002) mapped CH_3CN, and more recently, three compact cores, MM1, MM2, and MM3, were found in the 1.3 mm continuum map (Minh et al. 2010). The largest core, MM1, is about $3'' \times 6''$, and all three cores are covered by the CSO beam. The MM1 core was further resolved into two emission peaks, MM1a and MM1b, which present different chemical compositions (Minh et al. 2010). SO, SO_2, HCCCN, NH_2CHO, and HCOOH were detected in MM1a, whereas MM1b exhibits more COMs such as CH_3OH, $HCOOCH_3$, and C_2H_5OH. Other studies also reported COMs such as CH_3OH, CH_3CN, C_2H_5OH, $HCOOCH_3$, and *trans*-HCOOH (Menten et al. 1986; Pankonin et al. 2001; Minier & Booth 2002; Remijan et al. 2004a; Reiter et al. 2011).

We fitted CH_3OH, H_2CCO, CH_3CCH, CH_3CN, HCCCN, H_2CS, OCS, SO, and SO_2. Two CH_3OH temperature components are found, a cold one at 19 K and a warm one at 207 K. CH_3CN and SO_2 are above 100 K, and the rest of the molecules are below 100 K. The widths of the lines show two categories: CH_3CCH, cold CH_3OH, H_2CS, and SO are narrow, between 4.2 and 5.5 km s^{-1}; CH_3CN, warm CH_3OH, H_2CCO, HCCCN, OCS, and SO_2 are wide, between 7.4 and 10.2 km s^{-1}. The velocities are consistent within 1 km s^{-1}. No detection was found for $HCOOCH_3$, C_2H_5OH, NH_2CHO, and HCOOH, likely due to the heavy beam dilution effect. The asymmetric H_2CO $3_{1,2} \rightarrow 2_{1,1}$ line was modeled with two Gaussian components.

4.19. W51

W51 has two molecular cores, e1 and e2, and two extended continuum emission regions, IRS 1 and IRS 2 (Ho & Young 1996). We pointed to the center of e1, but also covered the entire e2 core with our CSO beam. Edges from IRS 1 may also be included in the beam. A spectral line survey of the e1 and e2 cores in the 3 mm band was reported by Kalenskii & Johansson (2010b), who detected COMs such as CH_3OH, CH_3CN, CH_3OCHO, C_2H_5OH, CH_3OCH_3, CH_3CH_2CN, CH_3COCH_3, and C_2H_5OOCH. They found that O-bearing molecules dominate the e2 core whereas N-bearing molecules dominate the e1 core. Other observations across the millimeter bands have detected multiple COMs, including CH_3OH, CH_3CN, CH_3CCH, $HCOOCH_3$ (g.s. and $v_t = 1$), $HCOO^{13}CH_3$, C_2H_5OH, CH_3CHO, c-C_2H_4O, *trans*-HCOOH, CH_3COOH, C_2H_5CN (g.s., $v_t = 1$, and $v_b = 1$), C_2H_3CN, and, tentatively, $(CH_2OH)_2$ (Dickens et al. 1997; Slysh et al. 1999; Kalenskii et al. 2000a, 2000b, 2002; Ikeda et al. 2001; Alakoz et al. 2002; Minier & Booth 2002; Remijan et al. 2002, 2008; Demyk et al. 2008; Jordan et al. 2008; Wirström et al. 2011; Favre et al. 2014; Hernández-Hernández et al. 2014; Lykke et al. 2015; Suzuki et al. 2016). The rotational temperatures of CH_3OH, CH_3CN, C_2H_5OH, and C_2H_3CN were derived to be above 150 K, whereas those of CH_3CHO and $HCOOCH_3$ were below 100 K (Ikeda et al. 2001; Remijan et al. 2002, 2004b).

We detected CH_3OH, $^{13}CH_3OH$, CH_3OCH_3, $HCOOCH_3$, H_2CCO, CH_3CCH, CH_3CN, CH_2NH, HCCCN, H_2CS, OCS, SO, and SO_2. Due to limited spectral sampling, the noise level above 259.5 GHz is noticeably higher than the rest of the spectrum. To avoid the unrealistic temperature simulations of large COMs from overfitting the noise in this spectral region, we truncated the molecular catalogs of CH_3OCH_3, $HCOOCH_3$, and H_2CCO at 259.5 GHz. Visual examinations confirmed that fits better matched the actual observed lines after this adjustment. The temperatures of the molecules in this source span a wide range from 14 to 472 K. The 472 K $HCOOCH_3$, in contrast to the result of Ikeda et al. (2001), appears to be much hotter than the rest of the molecules. Warm CH_3OH and CH_3CN are above 200 K, and CH_3OCH_3, $^{13}CH_3OH$, and SO_2 are above 100 K. The CH_3CN rotational temperature, 226 K, is slightly higher than that found by Remijan et al. (2002), which is not surprising because the 3 and 2 mm lines of CH_3CN showed a larger intensity scattering in the analysis of Remijan et al. (2002), likely due to the inconsistency of beam sizes. The cold CH_3OH component is at 23 K. The FWHMs of the molecules range from 7.5 to 11.4 km s^{-1}, and the velocities range from 1 to 4 km s^{-1}, redshifted. The asymmetric H_2CO $3_{1,2} \rightarrow 2_{1,1}$ line was modeled with two Gaussian components.

4.20. W3(H_2O)

W3 is a massive star-forming region with a hot core, W3(H_2O), indicated by the H_2O maser (Alcolea et al. 1993; Wilner et al. 1999), and an ultracompact H II region, W3(OH), which is indicated by the OH maser (Wyrowski et al. 1997). The OH maser is located 6″ to the west of W3(H_2O) (Turner & Welch 1984; Wilner et al. 1995). CH_3OH masers are also present in this region (Slysh et al. 1999). Our CSO beam covered both sources, but was centered on W3(H_2O).

Both cores have a rich inventory of COMs, revealed by extensive line surveys across the millimeter bands (Helmich et al. 1994; Helmich & van Dishoeck 1997; Kalenskii et al. 1997, 2000a; Wyrowski et al. 1999a; van der Tak et al. 2000; Ikeda et al. 2001; Alakoz et al. 2002; Charnley 2004; Sutton et al. 2004; Kim et al. 2006; Bisschop et al. 2007; Fontani et al. 2007; Ratajczak et al. 2011; Reiter et al. 2011; Li et al. 2012; Gerner et al. 2014; Hernández-Hernández et al. 2014; Ligterink et al. 2015; Qin et al. 2015). Detected COMs include CH_3OH, $^{13}CH_3OH$, C_2H_5OH, NH_2CHO, CH_3CN, $CH_3^{13}CN$, C_2H_5CN, C_2H_3CN, $HCOOCH_3$, CH_3OCH_3, H_2CCO, CH_3CHO, CH_3CCH, and *trans*-HCOOH, as well as ground state and vibrationally excited HCCCN. The rotational temperature of most COMs ranges between 100 and 250 K (Helmich & van Dishoeck 1997; Fontani et al. 2007; Qin et al. 2015), and CH_3OH has two temperature components (Qin et al. 2015). Cold CH_3OH, CH_3CCH, C_2H_5OH, and CH_3CHO lines were also observed at low frequency (3 mm and centimeter; Menten et al. 1986; Alakoz et al. 2002; Charnley 2004; Kim et al. 2006).

CH_3CN lines in the 1.3 mm band have been imaged to reveal the binary rotational structure of W3(H_2O) (Chen et al. 2006). The CH_3CN lines in W3(H_2O) have wide velocity range from −55 to −43 km s^{-1} (i.e., −8 to 4 km s^{-1} with respect to our v_{lsr}), whereas the CH_3CN lines in W3(OH) are more concentrated in the velocity channels from −48 to −43 km s^{-1} (−1 to 4 km s^{-1} with respect to our v_{lsr}).

In our survey, we fit CH_3OH, $^{13}CH_3OH$, CH_3OCH_3, H_2CCO, $HCOOCH_3$, CH_3CCH, CH_3CN, C_2H_5CN, HCCCN (both ground state and $v_7 = 1$), H_2CS, OCS, SO, and SO_2. The line shapes of the warm O-bearing molecules, including CH_3OH, $^{13}CH_3OH$, CH_3OCH_3, and $HCOOCH_3$, are asymmetric, and can be modeled with two velocity components. For each of these molecules, one component is redshifted from 1.7 to 2.5 km s^{-1} with a narrower FWHM between 4 and 5.8 km s^{-1}, while another component is blueshifted from 0 to 3.2 km s^{-1} with a wider FWHM between 5.4 and 9.7 km s^{-1}. Comparing this kinematic information to Chen et al. (2006), it is likely that the wide, blueshifted components arise from the W3(H_2O) region, and the redshifted, narrow components arise from the W3(OH) region. We found that the narrow components of CH_3OH, $^{13}CH_3OH$, CH_3OCH_3, and $HCOOCH_3$ are all hot, with rotational temperatures of 100–162 K. CH_3OH and CH_3OCH_3 from the W3(H_2O) region, on the other hand, have both hot (150–156 K) and cold (17–23 K) components. The SO_2 line profile is more complicated; it can be modeled with three components, each of which has a distinct rotational temperature (17, 70, and 148 K), velocity, and line width. It is difficult to attribute these components definitively to either the W3(H_2O) or the W3(OH) regions. These temperatures are comparable to the results from Helmich et al. (1994) and Bisschop et al. (2007). The temperatures of N-bearing molecules are slightly colder than the warm O-bearing molecules, ranging between 83 and 152 K. The asymmetric H_2CO $3_{1,2} \rightarrow 2_{1,1}$ line was modeled with three Gaussian components.

4.21. GAL 034.3+00.2

GAL 034.3+00.2 is a high-mass, chemically rich star-forming region with ultracompact H II regions (Benson & Johnston 1984) and embedded hot cores (Garay & Rodriguez 1990; Carral & Welch 1992). Numerous small molecules are present in this region (Macdonald et al. 1996), and multiple COMs have also been detected across the millimeter bands. The detected COMs include common interstellar O-bearing and N-bearing molecules such as CH_3OH, CH_3CCH, CH_3CN, C_2H_3CN, C_2H_5CN, NH_2CHO, C_2H_5OH, CH_3OCH_3, $HCOOCH_3$, $HCOOCH_3$, *trans*-HCOOH, CH_3CHO, and CH_3COOH (MacDonald et al. 1995; Millar et al. 1995; Macdonald et al. 1996; Mehringer & Snyder 1996; Dickens et al. 1997; Hatchell et al. 1998b; Nummelin et al. 1998b; Slysh et al. 1999; Watt & Mundy 1999; Kalenskii et al. 2000a, 2000b; Kim et al. 2000, 2001; Ikeda et al. 2001; Alakoz et al. 2002; Remijan et al. 2003; Charnley 2004; Mookerjea et al. 2007; Reiter et al. 2011; Rosero et al. 2013; Lykke et al. 2015; Fu & Lin 2016; Suzuki et al. 2016). Istopologues such as CH_2DCN and $^{13}CH_3OH$ are also observed (Gerin et al. 1992; Macdonald et al. 1996; Hatchell et al. 1998b).

GAL 034.3+00.2, is an incredibly rich source in chemistry. We were able to derive reliable rotational temperatures and densities for 22 molecules, in addition to the detection of spectral lines from 22 other small molecules and their isotopologues. In addition to the commonly detected CH_3OH, CH_3OCH_3, CH_3CCH, CH_3CN, H_2CCO, H_2CS, HCCCN, $HCOOCH_3$, OCS, SO, and SO_2, we found C_2H_3CN, C_2H_5CN, C_2H_5OH, CH_3CHO, CH_3COCH_3, NH_2CHO, CH_2NH, HCCCN ($v_7 = 1$), and *trans*-HCOOH. $^{13}CH_3OH$ and $^{13}CH_3CN$ are both detected. We did not analyze CH_3COOH because the available molecular catalog was incomplete. CH_3OH was fitted to two components, a cold one at 16 K and a warm one at 190 K. On the other hand, one component at 155 K was sufficient to describe $^{13}CH_3OH$. Other COMs have temperatures spanning 25 to 160 K. Surprisingly, CH_3OH, instead of CH_3CN, is the hottest molecule in GAL 034.3+00.2. The FWHMs are between 4 and 8 km s^{-1}. The velocities are consistent in the range of −1 and 1 km s^{-1}. The asymmetric H_2CO $3_{1,2} \rightarrow 2_{1,1}$ line was modeled with three Gaussian components.

4.22. GAL 31.41+0.31

GAL 31.41+0.31 is a high-mass star-forming region (Cesaroni et al. 1994) with embedded hot cores (Osorio et al. 2009; Cesaroni et al. 2011) and outflows (Maxia et al. 2001; Beltrán et al. 2004; Araya et al. 2008; Moscadelli et al. 2013). CH_3CN was used as a tracer for the structure and kinematics and extensively mapped in the millimeter (Olmi et al. 1995; Walmsley et al. 1995; Olmi et al. 1996a, 1996b; Pankonin et al. 2001; Beltrán et al. 2004, 2005; Araya et al. 2005; Purcell et al. 2006; Hernández-Hernández et al. 2014). Numerous COMs have been detected in this region via multiple millimeter and submillimeter line surveys. The detected COMs include CH_3OH, $^{13}CH_3OH$, CH_3CN, CH_3CCH, CH_3OCH_3, $HCOOCH_3$, C_2H_5OH, CH_3CHO, c-C_2H_4O, *trans*-HCOOH, C_2H_3CN, C_2H_5CN, and CH_3COCH_3 (Hatchell et al. 1998b;

Nummelin et al. 1998b; Ikeda et al. 2001; Fontani et al. 2007; Araya et al. 2008; Jordan et al. 2008; Beltrán et al. 2009; Reiter et al. 2011; Isokoski et al. 2013; Calcutt et al. 2014; Ligterink et al. 2015; Suzuki et al. 2016). It is one of the sources where CH_2OHCHO (glycolaldehyde), a sign of complex chemistry, was reported (Beltrán et al. 2009; Beltràn et al. 2010; Calcutt et al. 2014).

GAL 31.41+0.31 is one of the chemically richest sources in our list. We were able to derive reliable rotational temperature and density for 22 molecules, in addition to the detection of spectral lines from 19 other small molecules and their isotopologues. In addition to the commonly detected CH_3OH, CH_3OCH_3, CH_3CCH, CH_3CN, H_2CCO, H_2CS, HCCCN, $HCOOCH_3$, OCS, SO, and SO_2, we found C_2H_3CN, C_2H_5CN, C_2H_5OH, CH_3CHO, CH_3COCH_3, NH_2CHO, CH_2NH, and CH_3SH. ^{13}C isotopologues of CH_3OH and CH_3CN are also detected. The $^{13}CH_3OH$:CH_3OH ratio is 0.16, whereas the $^{13}CH_3CN$:CH_3CN ratio is 0.05. The temperatures of the COMs span 20 to 320 K. Both $^{13}CH_3OH$ and CH_3OH have two components, a cold one at ~40 K and a warm one above 200 K. The temperature of $^{13}CH_3CN$ is lower than that of CH_3CN, with the former at 105 K and the latter at 321 K. Additionally, CH_3CN ($v_8 = 1$) is detected at 180 K. The FWHMs of the lines are between 5 and 10 km s^{-1}. The asymmetric H_2CO $3_{1,2} \rightarrow 2_{1,1}$ line was modeled with three Gaussian components.

4.23. GAL 10.47+00.03

GAL 10.47+00.03 is an ultracompact H II region with an embedded hot core (Cesaroni et al. 1992; Pascucci et al. 2004). It is surprising that GAL 10.47+00.03 has chemical complexity comparable to that of Orion-KL. Hot cores have been identified in this UC H II region (Pascucci et al. 2004), and methyl cyanide (CH_3CN) (Olmi et al. 1993, 1995,1996a, 1996b; Araya et al. 2005; Hernández-Hernández et al. 2014) has been used to map this source. The molecular line surveys were conducted by a few groups (Hatchell et al. 1998b; Nummelin et al. 1998b; Ikeda et al. 2001; Pankonin et al. 2001; Hatchell & van der Tak 2003; Purcell et al. 2006; Fontani et al. 2007; Jordan et al. 2008; Rolffs et al. 2011). Detections of several COMs, including O-bearing molecules CH_3OH, $^{13}CH_3OH$, CH_3CCH, CH_3CHO, CH_3OCH_3, $HCOOCH_3$, CH_3CHO, CH_3COCH_3, *trans*-HCOOH, C_2H_5CN, C_2H_3CN, and NH_2CHO were reported in these surveys. Sulfur chemistry, probed by H_2CS, SO, and SO_2 emissions, was studied by Hatchell et al. (1998a). Suzuki et al. (2016) detected CH_2NH in this source as well.

In our survey, we report the rigorous detection of 13 COMs, in addition to 29 smaller molecules. For O-bearing molecules, we detected CH_3OH with a cold and a warm component, as well as $^{13}CH_3OH$, CH_3OCH_3, H_2CCO, $HCOOCH_3$, *trans*-HCOOH, C_2H_5OH, CH_3CHO, and CH_3COCH_3. For N-bearing molecules, we detected CH_3CN (both ground state and $v_8 = 1$), $^{13}CH_3CN$, C_2H_3CN, C_2H_5CN, CH_2NH, HCCCN, and NH_2CHO. Because of heavy line blending, the FWHMs of C_2H_5OH, CH_3CHO, and CH_3COCH_3 were fixed to 10 km s^{-1} for the fit to converge. Our result of detected COMs agrees well with previous line surveys. The cold CH_3OH component is at 21 K, while the warm component is at 258 K. All CH_3OH emission features could be modeled well with LTE. $HCOOCH_3$ is slightly colder than the warm CH_3OH at 233 K. Other O-bearing COMs are slightly colder than the warm CH_3OH, with $^{13}CH_3OH$ at 179 K, and CH_3OCH_3, H_2CCO, and *trans*-HCOOH all between 130 and 150 K, agreeing with the result for CH_3OCH_3 from Ikeda et al. (2001). The temperatures of N-bearing COMs span a wide range. Methyl cyanide is one of the hottest: the main species is at 668 K, the $v_8 = 1$ state is at 733 K, and the ^{13}C isotopologue is at 298 K. N-bearing COMs also suffer from a large temperature uncertainty due to heavy line blending. The methyl cyanide temperature is found to be much higher than the literature value of 148 K (Olmi et al. 1996b). In our survey, we observed emission features from methyl cyanide lines up to $K = 12$ in the $J = 12 \rightarrow 11$, $J = 13 \rightarrow 12$, and $J = 14 \rightarrow 13$ ladders. The higher K lines observed as compared to Olmi et al. (1996b) cause the higher rotational temperature of methyl cyanide in our analysis. CH_2NH is at 654 K, but with a large temperature uncertainty because of line blending. C_2H_3CN is much hotter than C_2H_5CN, the former being at 507 K, and the latter being at 177 K. NH_2CHO is at 248 K. For S-bearing molecules, we detected H_2CS, OCS, SO, and SO_2. They are significantly colder than the N-bearing species, with the hottest SO_2 at 162 K. CH_3CCH is also present in large abundance at a moderate temperature of 59 K.

The FWHMs of these molecular lines are relatively wide, spanning 7 to 12 km s^{-1}. The line shape is symmetric, agreeing with Olmi et al. (1993, 1996b). The asymmetric H_2CO $3_{1,2} \rightarrow 2_{1,1}$ line was modeled with two Gaussian components.

4.24. Orion-KL

The molecular lines and chemistry in Orion-KL have been extensively studied by numerous groups (Sutton et al. 1985, 1995; Menten et al. 1986; Blake et al. 1987; Turner 1989, 1991; Mangum et al. 1990; Minh et al. 1993; Groesbeck 1995; Dickens et al. 1997; Schilke et al. 1997, 2001; Slysh et al. 1999; Ikeda et al. 2001; Lee et al. 2001; Liu et al. 2001, 2002; Alakoz et al. 2002; Minier & Booth 2002; White et al. 2003; Beuther et al. 2004, 2006; Charnley 2004; Comito et al. 2005; Friedel et al. 2005; Persson et al. 2007; Friedel & Snyder 2008; Remijan et al. 2008; Goddi et al. 2009; Crockett et al. 2010; Gupta et al. 2010; Margulès et al. 2010; Favre et al. 2011a, 2011b; Zapata et al. 2011; Friedel & Widicus Weaver 2012; Brouillet et al. 2013; Crockett et al. 2014; Favre et al. 2014; Frayer et al. 2015; Morris et al. 2016; Suzuki et al. 2016; Tahani et al. 2016). We observed this source with a pointing centered on the Orion Hot Core as described by Blake et al. (1986). Due to the extreme complexity of the kinematics of Orion-KL, the line shapes are asymmetric and non-Gaussian. Our global fit for Orion-KL required more manual configuration for the fitting parameter space, and the overall fit residual was not as clean as the other sources we analyzed. For several molecules such as HCCCN, HCCCN ($v_7 = 1$), and CH_2NH, Gaussian components with fixed FWHM and δv were necessary to constrain the overall line shape of the transitions. There were also numerous lines that could not be modeled or were only partially modeled. Nonetheless, as a benchmark source, our detection of many COMs, including CH_3OH, $^{13}CH_3OH$, CH_3OCH_3, $HCOOCH_3$, CH_3COCH_3, *trans*-HCOOH, C_2H_3CN, C_2H_5CN, and CH_3CN, agrees with the previous literature. The asymmetric H_2CO $3_{1,2} \rightarrow 2_{1,1}$ line was modeled with three Gaussian components.

4.25. Sgr B2(N-LMH)

Sgr B2(N-LMH) is by far the most chemically complex source observed. A large portion of reported COMs were first detected in Sgr B2(N), which is known to harbor the largest number of COMs of any sightline investigated thus far. There are numerous literature studies of both comprehensive broadband line surveys and detailed studies for individual molecules for Sgr B2(N): to list a few, for example, Goldsmith & Linke (1981), Miao & Snyder (1997), Mehringer et al. (1997), Nummelin et al. (1998a, 2000), Cernicharo et al. (1999), Hollis et al. (2000, 2006), Liu et al. (2001), Snyder et al. (2002), Remijan et al. (2002), Halfen et al. (2006, 2011, 2013), Apponi et al. (2006), Requena-Torres et al. (2006), Belloche et al. (2007, 2008, 2009, 2013), Leigh et al. (2007), Halfen & Ziurys (2008), Remijan et al. (2008), Martín-Pintado et al. (2001), Friedel et al. (2004), Favre et al. (2014), and Neill et al. (2014). Because of the extreme spectral complexity and numerous previous studies that have targeted this source, we only provide the deconvolved spectrum of Sgr B2 (N-LMH) without performing a global spectral analysis.

5. Discussion

Given that this set of sources was targeted because they are known to be rich in COMs, it does not come as a surprise that many of these sources have extremely rich chemistry. This chemical richness means that trends that offer insight into chemical pathways that have long been assumed for star-forming regions can be discerned. An overview of the results in graphical form is given in Figure 3. Here we plot the column density for a given molecule as a circle. The area of each circle is scaled to the magnitude of the column density. The color of each circle corresponds to the temperature, the scale for which is shown on the right. Sources are sorted on the horizontal axis by type, and within each type the chemical complexity of the sources is arranged to increase from left to right. The molecules are sorted on the vertical axis, grouped into the O-bearing, N-bearing, and S-bearing species. Within each group, molecules on the top are more frequently detected in the sources. As such, trends are easily discernible in the data set. For molecules with multiple temperature and velocity components, we plot concentric circles with each ring representing one component. The column density of molecules in Orion-KL was divided by 10 before plotting.

Here we will not attempt a detailed discussion of each molecule detected in each source and the corresponding implications, but rather will save that level of detail for subsequent papers that examine a particular chemical or physical subset from this data set. Nonetheless, we can immediately find general trends in these results that offer glimpses into the power of such comprehensive observational studies. The most striking features of these results as gleaned from Figure 3 are as follows:

1. Although most sources are chemically complex, this is not universally true. Among different source types, hot cores present the most complex chemistry, indicated by the large number of COMs observed in these sources. Protostars present some level of complexity. Hot corinos are quiet in this survey, likely due to their small source sizes and therefore severe beam dilution effect. Some observed complexity is expected, given that these sources were chosen because COMs had already been detected in previous observations. But the level of complexity in some of these sources is comparable to that of Orion-KL. The most striking case is that of GAL 10.47+00.03, which displays a remarkable array of COMs.
2. Methanol, CH_3CCH, H_2CS, OCS, SO, and SO_2 are nearly ubiquitous in this sample set. Methanol, SO, and SO_2 are known to be indicators of grain mantle disruption (Charnley 1997; Hatchell et al. 1998a; Buckle & Fuller 2003), hence it is possible that these other ubiquitous molecules are also indicators of this process. It is particularly noteworthy that all of the major sulfur-bearing species are on this list.
3. CH_3OH is ubiquitous, as is expected. For most hot cores, two CH_3OH temperature components can usually be found: a cold one of 10–30 K and a warm one ranging from 100 to 300 K. The temperature of the warm CH_3OH appears to be a variable dependent on the size and evolutionary stage of the central star. The difference between the temperatures for cold and warm methanol is significant. Since methanol is abundant, its line opacity may introduce systematic error in the rotational temperature values determined under the optically thin assumption. Nevertheless, the line shapes for the methanol lines we observed are Gaussian, indicating that the lines are not completely opaque. Based on our beam-averaged results, the cold methanol component usually has a maximum optical depth (τ) value of 0.1–0.5, while the warm component has a τ on the order of 0.01. If beam dilution was considered, the τ value would be higher, which could make the strongest cold methanol lines marginally optically thick. But overall this will not change the qualitative result that two methanol temperatures coexist in our sources. The observation of two methanol temperature components is also supported by results in the literature, i.e., in Orion-KL (Blake et al. 1986) and G31.41 (Isokoski et al. 2013). $^{13}CH_3OH$ was only detected in massive star-forming regions with a high CH_3OH abundance.
4. CH_3CCH is nearly as ubiquitous and abundant as CH_3OH, and it is always cold compared to other COMs that were detected. This may indicate that the emission of CH_3CCH arises from the extended envelope around the hot cores. CH_3CCH is highly abundant, on the same order of magnitude as CH_3OH. CH_3CCH, as a small carbon chain molecule, is thought to be a tracer for the cold chemistry in dense clouds (Kuiper et al. 1984). A "warm carbon chain chemistry" (WCCC; Sakai et al. 2008) was proposed to explain the detection of carbon chains, including CH_3CCH, in several envelopes of low-mass star-forming regions with a moderate temperature around 30 K (Sakai et al. 2008, 2009a, 2009b). The prevalence of CH_3CCH in all of the hot cores may be support for this WCCC, where regeneration mechanisms of the carbon chain molecules during the warm-up phase may be important (Hassel et al. 2011). Further studies of the formation mechanisms of CH_3CCH around hot cores are warranted.
5. The S-bearing molecules, H_2CS, OCS, SO, and SO_2 are nearly ubiquitous in this sample set, which is to be expected since they are structurally simpler than COMs, and therefore have stronger spectral lines. S-bearing molecules are proposed to be indicators of grain mantle

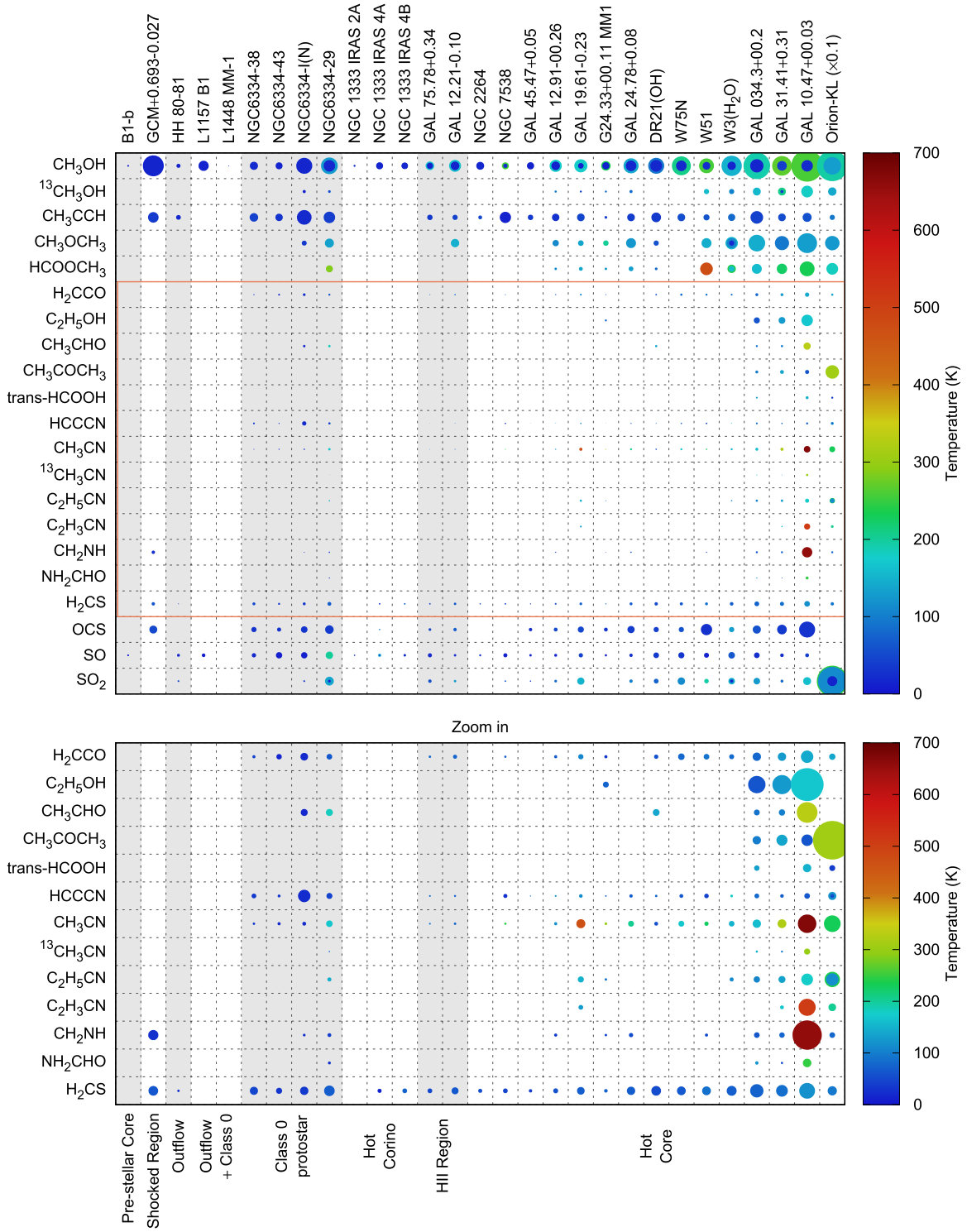

Figure 3. Visualization of Table 3: column density and LTE temperature. Sources are on the horizontal axis, and molecules are on the vertical axis. The areas of the circles are proportional to the column density of the molecules. The circles for Orion-KL are decreased by a factor of 10 in area to fit the overall scale of the plot. For molecules with multiple temperature components, concentric circles are drawn, where each ring represents one component. The color of the circles indicates the LTE temperature of the molecules, with the scale given to the right. The full-scale plot is presented in the top panel, and the zoomed-in region, highlighted by the orange frame, is presented in the bottom panel.

disruption and material injection into the gas phase during the star formation process, and therefore can be used as a chemical clock to trace the evolutionary stage of the source (Charnley 1997; Hatchell et al. 1998a; Buckle & Fuller 2003). However, Wakelam et al. (2004) argued that this chemical clock approach is not straightforward.

In our surveys, SO is always present. SO and OCS are definitively detected in Orion-KL, but not included in Figure 3 because the narrower spectral coverage for Orion-KL provides insufficient information to perform LTE analysis on these molecules. H_2CS correlates well with SO across our sources, while OCS and SO_2 do not

always coexist. In NGC 1333 IRAS 4A, NGC 6334–38, NGC 6334–43, and G24.33+00.11 MM1, we have only detected OCS but not SO_2. Since SO_2 is generally less abundant than OCS and SO in other sources, the non-detection of SO_2 in NGC 1333 IRAS 2A may simply be caused by its low line intensity, which is below our detection limit. NGC 6334–38, NGC 6334–43, and G24.33+00.11 MM1, however, display significant OCS abundances. In HH 80–81 and NGC 7538, we only detect SO_2 and not OCS. For sources where all four S-bearing molecules are detected, the abundance ratios vary dramatically from source to source. For example, GAL 10.47+00.03 and W51, compared to other hot cores, have significantly more OCS than the rest of the S-bearing molecules. Orion-KL is the anomaly on the other extreme: it has an extensive amount of SO_2, which is as abundant as CH_3OH. In general, we conclude that the abundance of S-bearing small molecules cannot be explained by a simple correlation with the evolutionary stage of the star-forming region. Our observations agree with the argument addressed by Wakelam et al. (2004).

6. Nearly all molecules detected that have a CN group are found at elevated temperatures relative to O-bearing COMs. Despite the prevalence of these species in these sources, they are present at much lower abundances than their O-bearing counterparts. The variation of the CH_3CN temperature across sources is also large. Unlike CH_3CCH, which is always cold, or CH_3OCH_3 and $HCOOCH_3$, which are always warm but only present in chemically evolved sources, CH_3CN is detected in nearly every source, and its temperature correlates with the source type. C_2H_3CN and C_2H_5CN, two "interstellar weeds" thought to be ubiquitous in the ISM, are only detected in a handful of massive star-forming regions with the richest chemistry and most elevated temperatures (Crockett et al. 2014). It could be that the cyanides larger than CH_3CN are both warm and compact, and therefore beam diluted beyond the point of detection here. The abundance of C_2H_5CN is low relative to CH_3CN, despite their nearly equal abundance in Orion-KL.
7. There may be a chemical link between dimethyl ether (CH_3OCH_3) and methyl formate ($HCOOCH_3$) through grain-surface chemistry (see Garrod et al. 2008 for a detailed discussion). However, these two molecules do not display obvious trends in abundance or temperature. In general, CH_3OCH_3 is more abundant and colder than $HCOOCH_3$, but the ratio between the CH_3OCH_3 and $HCOOCH_3$ column densities is not consistent throughout our sample set. This result is unexpected, given that they are both presumed to form from grain-surface processes involving the CH_3O radical. The model by Garrod & Widicus Weaver (2013) showed that the abundances of CH_3OCH_3 and $HCOOCH_3$ peak at different temperatures during the warm-up phase, and their peak abundance is largely affected by the warm-up speed. In a fast warm-up period, $HCOOCH_3$ has a higher peak abundance than that of CH_3OCH_3. In contrast, in a medium or slow warm-up period, CH_3OCH_3 has a higher peak abundance than that of $HCOOCH_3$. In addition, beam dilution can contribute to this inconsistency if CH_3OCH_3 and $HCOOCH_3$ have different spatial distributions. It is unclear if scaling by the spatial scale of the emission would result in column densities that are correlated; additional interferometric observations are warranted. Nevertheless, if the model (Garrod & Widicus Weaver 2013) is correct, the abundance ratio between CH_3OCH_3 and $HCOOCH_3$ may then probe the warm-up speed of hot cores.
8. Previous interferometric studies of $HCOOCH_3$ in Orion indicated that it is formed on grain surfaces and detected in the colder, extended regions rather than in the hot core (Friedel & Widicus Weaver 2012; Favre et al. 2014). In our results, however, $HCOOCH_3$ is shown to be present at warmer temperatures than CH_3OCH_3 and most of the other O-bearing COMs that are detected. This result is consistent with the findings in other massive star-forming regions such as GAL 24.78, GAL 75.78, W3(H_2O), and GAL 12.91 (Bisschop et al. 2007; Isokoski et al. 2013). In these surveys, dimethyl ether is consistently found at temperatures lower than 150 K, while the temperature of methyl formate is consistently higher than that of dimethyl ether. In Sgr B2(N), however, Belloche et al. (2013) detected dimethyl ether at 130 K and methyl formate at 80 K. Our results agree with Bisschop et al. (2007) and Isokoski et al. (2013), but the reason for this trend and the reason for Sgr B2(N) being an outlier are unclear. It is possible that we could sufficiently describe the $HCOOCH_3$ spectral intensity with one temperature component due to its weaker overall line intensities, and this temperature is in fact an average of two different temperatures. If a warm component can be found in multiple sources, it is not impossible that the gas-phase formation mechanisms for $HCOOCH_3$ (Horn et al. 2004) are still relevant, although they do not account for all of the observed $HCOOCH_3$ abundance. Further interferometric investigation of the $HCOOCH_3$ spatial distribution as a function of temperature in sources other than Orion-KL is warranted.
9. Complex O-bearing species such as C_2H_5OH, CH_3CHO, *trans*-HCOOH, and NH_2CHO are not highly abundant in these sources. They are only detected in a few sources. Indeed, complex molecules are more difficult to detect, because of their weaker line intensities and their lower abundances. But our result has implications on the possibility of more complex chemistry, as many of these species are thought to be chemical precursors to more complex molecules. If these molecules are even less abundant than what was anticipated before, the formation routes for more complex molecules are uncertain.
10. Interstellar acetone has previously only been detected in Sgr B2 (N-LMH) (Snyder et al. 2002), Orion-KL (Friedel et al. 2005), GAL 10.47+00.03 (Rolffs et al. 2011), and GAL 31.41+0.31 (Isokoski et al. 2013). We have confirmed the detections in Orion, GAL 10.47+00.03, and GAL 31.41+0.31 with a full-band analysis, and also detected acetone in GAL 034.3+00.2. An additional paper offering the details of the acetone analysis in these surveys is in preparation (L. Zou & S. L. Widicus Weaver 2017, in preparation).
11. The complexity of chemistry may not be directly correlated with elevated temperature. NGC 6334–29 and NGC 6334-I (N) have similar chemistry, but NGC 6334-I(N) is significantly colder than NGC 6334–29. In NGC 6334-I(N), CH_3OCH_3 and CH_3CHO are present at 35 K and 20 K, respectively. In NGC 6334–29, CH_3OCH_3 and CH_3CHO

are present at 135 K and 182 K, respectively. The cold CH_3OCH_3 and CH_3CHO indicate the possible grain-surface chemistry origin of these O-bearing molecules, but what unique process causes their sublimation into the gas phase in NGC 6334-I(N) in such a cold environment is not clear. Likewise, GAL 034.3+0.02 presents similar chemical complexity to GAL 31.41+0.31, but its average COM temperature is lower.

12. The non-LTE CH_3OH emissions, $8_{-1,8} \rightarrow 7_{0,7}$ (E_{low} = 78 K) at 229.76 GHz and $11_{0,11} \rightarrow 10_{1,10}$ (E_{low} = 141 K) at 250.51 GHz, are found primarily in shocks and H II regions. The $8_{-1,8} \rightarrow 7_{0,7}$ line can be modeled by our LTE fit only in W3(H_2O), GAL 034.3+0.02, GAL 31.41 + 0.31, GAL 10.47+00.03, and Orion-KL. These sources seem to be the richest sources in chemistry. The elevated methanol temperature in these sources may contribute to the flux of this warm methanol line. The $11_{0,11} \rightarrow 10_{1,10}$ lines can be modeled by our LTE fit only in GAL 75.78 + 0.34 and GAL 10.47+00.03, and the emission does not appear in B1-b, L1448 MM-1, or NGC 1333 IRAS 2A; in G24.33+00.11 MM1. In all other sources, they are observed in fluxes much larger than the CH_3OH simulation with the LTE model.

    Several postulations may explain these unexpected emissions, but more evidence is needed to support any of these postulations. The two methanol lines may overlap with the lines from another unknown molecular carrier, but searches in the molecular line databases did not return likely molecular candidates; these lines are not included because of interference with spectral artifacts. It is not likely that these two lines arise from an extended source in the line of sight of our target source, as they would usually have distinctive velocities that can be resolved in our surveys. The lower state energies of these two lines are also not extremely cold, which means that they are not likely to be emitted by some unknown methanol source under LTE, as one would expect to see more methanol lines in our spectral coverage with detectable intensities under this LTE temperature.

6. Conclusion

We conducted broadband CSO spectral line surveys of 30 star-forming regions in the 1.3 mm band (220–267 GHz). The deconcolved spectra are presented. For each spectrum, we performed a global LTE analysis for molecules with a sufficient number of spectral lines and intensities, using the GOBASIC program. Some molecular tracers, such as CH_3OH, CH_3CCH, and SO, are ubiquitously detected in these sources. The difference in chemical complexity between hot cores, hot corinos, and Class 0 protostars is verified. Within each type of star-forming region, however, unexpected variations in the molecular complexity, abundance, and temperatures, are present. No straightforward correlations between different COMs can be drawn, as it seems that each source demonstrates a unique chemistry. Because of the large size of the single-dish beam, line intensities are diluted, and spatial distributions of different molecules cannot be resolved. To reveal the details of the astrochemistry in these star-forming regions, more information from interferometric studies on these sources is required so that source size can be properly included in the analysis.

Support for this work was provided in part by the National Science Foundation CAREER Award CHE-1150492. Support for the development of GOBASIC was provided by NASA *Herschel* OT1 Analysis Program RSA No. 1428755, the Emory Chemistry Early Career Research Grant, Emory SURE and SIRE programs (funding from Howard Hughes Medical Institute grant No. 52005873), and the Emory College Undergraduate Research Matching Grant. S.L.W.W., J.C.L., L.Z., B.M.H., N.W., and B.A.M. were supported for this work by S. L.W.W.'s startup funds, provided by Emory University. J.L.S., M.L.R., T.N.C., and J.A.K. were also supported by S.L.W.W.'s Emory startup funds, and by the Emory SURE and SIRE programs (funding from Howard Hughes Medical Institute grant No. 52005873). B.A.M. is a Jansky Fellow of the National Radio Astronomy Observatory, which is a facility of the National Science Foundation operated under cooperative agreement by Associated Universities, Inc. D.C.L. acknowledges support by NASA (*Herschel* OT funding) through an award issued by JPL/Caltech. We thank Frank Rice, Jonas Zmuidzinas, and Geoffrey Blake for technical support with the prototype receiver and assistance in data collection for the Orion-KL spectrum. We thank Martin Emprechtinger, Peter Schilke, and Claudia Comito for helpful discussions regarding the analysis of line surveys and deconvolution of DSB spectra, Thomas Anderson for assistance during part of the observations, Gordon Stacey for collegiality with time-sharing the telescope during rapid weather transitions on Maunakea, and Thomas Phillips for his general guidance and support. We gratefully acknowledge the support and services offered by the CSO technical and support staff, in particular Simon Radford, Richard Chamberlin, Ed Bufil, Brian Force, Hiroshige Yoshida, and Diana Bisel. We also thank the support staff from Caltech and Emory. This material is based upon work performed at the Caltech Submillimeter Observatory, which was operated by the California Institute of Technology under cooperative agreement with the National Science Foundation (AST-0838261).

Software: GOBASIC (version 5.0), Rad et al. (2016), CLASS (versions jun13a and jul14a) , (GILDAS 2017).

ORCID iDs

Jacob C. Laas https://orcid.org/0000-0001-6876-6940
Dariusz C. Lis https://orcid.org/0000-0002-0500-4700
Brett A. McGuire https://orcid.org/0000-0003-1254-4817

References

Alakoz, A. V., Kalenskii, S. V., Promislov, V. G., Johansson, L. E. B., & Winnberg, A. 2002, ARep, 46, 551
Alcolea, J., Menten, K. M., Moran, J. M., & Reid, M. J. 1993, in The Proper Motions of the H_2O Masers Near W3(OH), ed. A. W. Clegg & G. E. Nedoluha (Berlin: Springer), 225
Angerhofer, P. E., Rossano, G. S., & Vestrand, W. T. 1978, AJ, 83, 1417
Apponi, A. J., Halfen, D. T., Ziurys, L. M., et al. 2006, ApJL, 643, L29
Araya, E., Hofner, P., Kurtz, S., Bronfman, L., & DeDeo, S. 2005, ApJS, 157, 279
Araya, E., Hofner, P., Kurtz, S., Olmi, L., & Linz, H. 2008, ApJ, 675, 420
Araya, E. D., Kurtz, S., Hofner, P., & Linz, H. 2009, ApJ, 698, 1321
Arce, H. G., Santiago-García, J., Jørgensen, J. K., Tafalla, M., & Bachiller, R. 2008, ApJL, 681, L21
Avery, L. W., & Chiao, M. 1996, ApJ, 463, 642
Bachiller, R., André, P., & Cabrit, S. 1991, A&A, 241, L43
Bachiller, R., Codella, C., Colomer, F., Liechti, S., & Walmsley, C. M. 1998, A&A, 335, 266
Bachiller, R., & Gutiérrez, M. P. 1997, ApJL, 487, L93

Bachiller, R., Pérez Gutiérrez, M., Kumar, M. S. N., & Tafalla, M. 2001, A&A, 372, 899
Belloche, A., Comito, C., Hieret, C., et al. 2007, in Molecules in Space and Laboratory, J.L. Lemaire & F. Combes (Paris: S. Diana), 10
Belloche, A., Garrod, R. T., Müller, H. S. P., et al. 2009, A&A, 499, 215
Belloche, A., Menten, K. M., Comito, C., et al. 2008, A&A, 482, 179
Belloche, A., Müller, H. S. P., Menten, K. M., Schilke, P., & Comito, C. 2013, A&A, 559, A47
Beltrán, M. T., Cesaroni, R., Codella, C., et al. 2006, Natur, 443, 427
Beltrán, M. T., Cesaroni, R., Neri, R., et al. 2004, ApJL, 601, L187
Beltrán, M. T., Cesaroni, R., Neri, R., et al. 2005, A&A, 435, 901
Beltrán, M. T., Cesaroni, R., Neri, R., & Codella, C. 2011, A&A, 525, A151
Beltrán, M. T., Codella, C., Viti, S., Neri, R., & Cesaroni, R. 2009, ApJL, 690, L93
Beltràn, M. T., Codella, C., Viti, S., Neri, R., & Cesaroni, R. 2010, HiA, 15, 701
Benedettini, M., Busquet, G., Lefloch, B., et al. 2012, A&A, 539, L3
Benson, J. M., & Johnston, K. J. 1984, ApJ, 277, 181
Bergin, E. A., & Tafalla, M. 2007, ARA&A, 45, 339
Beuther, H., Zhang, Q., Greenhill, L. J., et al. 2004, ApJL, 616, L31
Beuther, H., Zhang, Q., Reid, M. J., et al. 2006, ApJ, 636, 323
Bisschop, S. E., Jørgensen, J. K., van Dishoeck, E. F., & de Wachter, E. B. M. 2007, A&A, 465, 913
Blake, G. A., Masson, C. R., Phillips, T. G., & Sutton, E. C. 1986, ApJS, 60, 357
Blake, G. A., Sandell, G., van Dishoeck, E. F., et al. 1995, ApJ, 441, 689
Blake, G. A., Sutton, E., Masson, C., & Phillips, T. 1987, ApJ, 315, 621
Bottinelli, S., Ceccarelli, C., Lefloch, B., et al. 2004, ApJ, 615, 354
Bottinelli, S., Ceccarelli, C., Williams, J. P., & Lefloch, B. 2007, A&A, 463, 601
Brogan, C. L., Hunter, T. R., Cyganowski, C. J., et al. 2009, ApJ, 707, 1
Brouillet, N., Despois, D., Baudry, A., et al. 2013, A&A, 550, A46
Buckle, J. V., & Fuller, G. A. 2003, A&A, 399, 567
Buizer, J. M. D., & Minier, V. 2005, ApJL, 628, L151
Burkhardt, A. M., Dollhopf, N. M., Corby, J. F., et al. 2016, ApJ, 827, 21
Busquet, G., Lefloch, B., Benedettini, M., et al. 2014, A&A, 561, A120
Calcutt, H., Viti, S., Codella, C., et al. 2014, MNRAS, 443, 3157
Carral, P., & Welch, W. J. 1992, ApJ, 385, 244
CDMS 2017, Cologne Database for Molecular Spectroscopy, Universität zu Köln. http://www.astro.uni-koeln.de/cdms/
Cernicharo, J., Cox, P., Fossé, D., & Güsten, R. 1999, A&A, 351, 341
Cernicharo, J., Marcelino, N., Roueff, E., et al. 2012, ApJL, 759, L43
Cesaroni, R., Beltrán, M. T., Zhang, Q., Beuther, H., & Fallscheer, C. 2011, A&A, 533, A73
Cesaroni, R., Codella, C., Furuya, R. S., & Testi, L. 2003, A&A, 401, 227
Cesaroni, R., Hofner, P., Araya, E., & Kurtz, S. 2010, A&A, 509, A50
Cesaroni, R., Olmi, L., Walmsley, C. M., Churchwell, E., & Hofner, P. 1994, ApJL, 435, L137
Cesaroni, R., Walmsley, C. M., & Churchwell, E. 1992, A&A, 256, 618
Chandler, C. J., Moore, T. J. T., Mountain, C. M., & Yamashita, T. 1993, MNRAS, 261, 694
Charnley, S. 2004, AdSpR, 33, 23
Charnley, S. B. 1997, ApJ, 481, 396
Chen, H.-R., Welch, W. J., Wilner, D. J., & Sutton, E. C. 2006, ApJ, 639, 975
Choi, M., Tatematsu, K., & Kang, M. 2010, ApJL, 723, L34
Codella, C., Benedettini, M., Beltrán, M. T., et al. 2009, A&A, 507, L25
Codella, C., Ceccarelli, C., Lefloch, B., et al. 2012, ApJL, 757, L9
Codella, C., Lefloch, B., Ceccarelli, C., et al. 2010, A&A, 518, L112
Comito, C., Schilke, P., Phillips, T. G., et al. 2005, ApJS, 156, 127
Coutens, A., Persson, M. V., Jørgensen, J. K., Wampfler, S. F., & Lykke, J. M. 2015, A&A, 576, A5
Coutens, A., Vastel, C., Cabrit, S., et al. 2013, A&A, 560, A39
Crampton, D., Georgelin, Y. M., & Georgelin, Y. P. 1978, A&A, 66, 1
Crockett, N. R., Bergin, E. A., Neill, J. L., et al. 2014, ApJ, 787, 112
Crockett, N. R., Bergin, E. A., Wang, S., et al. 2010, A&A, 521, L21
Cuadrado, S., Goicoechea, J. R., Roncero, O., et al. 2016, A&A, 596, L1
Cunningham, N., Lumsden, S. L., Cyganowski, C. J., Maud, L. T., & Purcell, C. 2016, MNRAS, 458, 1742
Cyganowski, C. J., Whitney, B. A., Holden, E., et al. 2008, AJ, 136, 2391
de la Fuente, E., Kurtz, S. E., Rodriguez-Rico, C. A., et al. 2010, in IAU Symp. 262, Stellar Populations-Planning for the NExt Decade, ed. G. R. Bruzual & S. Charlot (Cambridge: Cambridge Univ. Press), 319
De Simone, M., Codella, C., Testi, L., et al. 2017, A&A, 599, A121
Demyk, K., Wlodarczak, G., & Carvajal, M. 2008, A&A, 489, 589
Dickens, J. E., Irvine, W. M., DeVries, C. H., & Ohishi, M. 1997, ApJ, 479, 307
Faúndez, S., Bronfman, L., Garay, G., et al. 2004, A&A, 426, 97
Favre, C., Carvajal, M., Field, D., et al. 2014, ApJS, 215, 25
Favre, C., Despois, D., Brouillet, N., et al. 2011a, A&A, 532, A32
Favre, C., Wootten, H. A., Remijan, A. J., et al. 2011b, ApJL, 739, L12
Fernández-López, M., Curiel, S., Girart, J. M., et al. 2011, ApJ, 141, 72
Fish, V. L., Muehlbrad, T. C., Pratap, P., et al. 2011, ApJ, 729, 14
Flower, D. R., Pineau des Forts, G., & Rabli, D. 2010, MNRAS, 409, 29
Fontani, F., Pascucci, I., Caselli, P., et al. 2007, A&A, 470, 639
Frayer, D. T., Maddalena, R. J., Meijer, M., et al. 2015, AJ, 149, 162
Friedel, D. N., & Snyder, L. E. 2008, ApJ, 672, 962
Friedel, D. N., Snyder, L. E., Remijan, A. J., & Turner, B. E. 2005, ApJL, 632, L95
Friedel, D. N., Snyder, L. E., Turner, B. E., & Remijan, A. 2004, ApJ, 600, 234
Friedel, D. N., & Widicus Weaver, S. L. 2012, ApJS, 201, 17
Fu, L., & Lin, G.-M. 2016, RAA, 16, 182
Furuya, R. S., Cesaroni, R., Codella, C., et al. 2002, A&A, 390, L1
Furuya, R. S., Cesaroni, R., & Shinnaga, H. 2011, A&A, 525, A72
Furuya, R. S., Cesaroni, R., Takahashi, S., et al. 2005, ApJ, 624, 827
Galván-Madrid, R., Zhang, Q., Keto, E., et al. 2010, ApJ, 725, 17
Garay, G., & Rodriguez, L. F. 1990, ApJ, 362, 191
Garrod, R. T., Weaver, S. L. W., & Herbst, E. 2008, ApJ, 682, 283
Garrod, R. T., & Widicus Weaver, S. L. 2013, ChRv, 113, 8939
Geppert, W. D., Hamberg, M., Thomas, R. D., et al. 2006, FaDi, 133, 177
Gerin, M., Combes, F., Wlodarczak, G., et al. 1992, A&A, 259, L35
Gerner, T., Beuther, H., Semenov, D., et al. 2014, A&A, 563, A97
Gezari, D. Y. 1982, ApJL, 259, L29
GILDAS 2017, GILDAS, Institut de Radioastronomie Millimétrique. http://www.iram.fr/IRAMFR/GILDAS/
Ginsburg, A., Bressert, E., Bally, J., & Battersby, C. 2012, ApJL, 758, L29
Girart, J. M., Frau, P., Zhang, Q., et al. 2013, ApJ, 772, 69
Goddi, C., Greenhill, L. J., Humphreys, E. M. L., et al. 2009, ApJ, 691, 1254
Goldsmith, P. F., & Linke, R. A. 1981, ApJ, 245, 482
Gómez, Y., Rodríguez, L. F., Girart, J. M., Garay, G., & Martí, J. 2003, ApJ, 597, 414
Gómez-Ruiz, A. I., Hirano, N., Leurini, S., & Liu, S.-Y. 2013, A&A, 558, A94
Gregersen, E. M., Evans II, N. J., Zhou, S., & Choi, M. 1997, ApJ, 484, 256
Groesbeck, T. D. 1995, PhD thesis, California Institute of Technology
Gupta, H., Rimmer, P., Pearson, J. C., et al. 2010, A&A, 521, L47
Halfen, D. T., Apponi, A. J., Woolf, N., Polt, R., & Ziurys, L. M. 2006, ApJ, 639, 237
Halfen, D. T., Ilyushin, V., & Ziurys, L. M. 2011, ApJ, 743, 60
Halfen, D. T., Ilyushin, V. V., & Ziurys, L. M. 2013, ApJ, 767, 66
Halfen, D. T., & Ziurys, L. M. 2008, in IAU Symp. 251, Organic Matter in Space (Cambridge: Cambridge Univ. Press), 27
Hassel, G. E., Harada, N., & Herbst, E. 2011, ApJ, 743, 182
Hatchell, J., Thompson, M. A., Millar, T. J., & MacDonald, G. 1998a, A&A, 338, 713
Hatchell, J., Thompson, M. A., Millar, T. J., & Macdonald, G. H. 1998b, A&AS, 133, 29
Hatchell, J., & van der Tak, F. F. S. 2003, A&A, 409, 589
He, J. H., Takahashi, S., & Chen, X. 2012, ApJS, 202, 1
Helmich, F. P., Jansen, D. J., de Graauw, T., Groesbeck, T. D., & van Dishoeck, E. F. 1994, A&A, 283, 626
Helmich, F. P., & van Dishoeck, E. F. 1997, A&AS, 124, 205
Herbst, E., & van Dishoeck, E. F. 2009, ARA&A, 47, 427
Hernández-Hernández, V., Zapata, L., Kurtz, S., & Garay, G. 2014, ApJ, 786, 38
Hirota, T., Bushimata, T., Choi, Y. K., et al. 2008, PASJ, 60, 37
Hirota, T., Honma, M., Imai, H., et al. 2011, PASJ, 63, 1
Ho, P. T. P., & Young, L. M. 1996, ApJ, 472, 742
Hofner, P., Peterson, S., & Cesaroni, R. 1999, ApJ, 514, 899
Hollis, J. M., Lovas, F. J., & Jewell, P. R. 2000, ApJL, 540, L107
Hollis, J. M., Lovas, F. J., Remijan, A. J., et al. 2006, ApJL, 643, L25
Horn, A., Möllendal, H., Sekiguchi, O., et al. 2004, ApJ, 611, 605
Horn, J., Siebertz, O., Schmülling, F., et al. 1999, ExA, 9, 17
Hunter, T. R., Brogan, C. L., Megeath, S. T., et al. 2006, ApJ, 649, 888
Ikeda, M., Ohishi, M., Nummelin, A., et al. 2001, ApJ, 560, 792
Isokoski, K., Bottinelli, S., & van Dishoeck, E. F. 2013, A&A, 554, A100
Jordan, E., Araya, E., Hofner, P., Mateen, M., & Kurtz, S. 2008, RMxAA, 44, 45
Jørgensen, J. K., Bourke, T. L., Myers, P. C., et al. 2005a, ApJ, 632, 973
Jørgensen, J. K., Bourke, T. L., Myers, P. C., et al. 2007, ApJ, 659, 479
Jørgensen, J. K., Hogerheijde, M. R., Blake, G. A., et al. 2004, A&A, 415, 1021
Jørgensen, J. K., Schöier, F. L., & van Dishoeck, E. F. 2005b, A&A, 437, 501

Kalenskii, S., Promislov, V., Alakoz, A., Winnberg, A., & Johansson, L. E. 2000a, A&A, 354, 1036
Kalenskii, S. V., Dzura, A. M., Booth, R. S., Winnberg, A., & Alakoz, A. V. 1997, A&A, 321, 311
Kalenskii, S. V., & Johansson, L. E. B. 2010a, ARep, 54, 295
Kalenskii, S. V., & Johansson, L. E. B. 2010b, ARep, 54, 1084
Kalenskii, S. V., Promislov, V. G., Alakoz, A. V., Winnberg, A., & Johansson, L. E. B. 2000b, ARep, 44, 725
Kalenskii, S. V., Slysh, V. I., & Val'tts, I. E. 2002, ARep, 46, 96
Kaul, A. B., Bumble, B., Lee, K. A., et al. 2004, JVSTB, 22, 2417
Kim, H.-D., Cho, S.-H., Chung, H.-S., et al. 2000, ApJS, 131, 483
Kim, H.-D., Cho, S.-H., Lee, C.-W., & Burton, M. 2001, JKAS, 34, 167
Kim, S.-J., Kim, H.-D., Lee, Y., et al. 2006, ApJS, 162, 161
Klein, B., Philipp, S. D., Krämer, I., et al. 2006, A&A, 454, L29
Knee, L. B. G., & Sandell, G. 2000, A&A, 361, 671
Kooi, J. W., Kovacs, A., Sumner, M. C., et al. 2007, ITMTT, 55, 2086
Kraus, S., Balega, Y., Elitzur, M., et al. 2006, A&A, 455, 521
Kuiper, T. B. H., Kuiper, E. N. R., Dickinson, D. F., Turner, B. E., & Zuckerman, B. 1984, ApJ, 276, 211
Kurtz, S. 2005, in IAU Symp. 227, Massive star birth: A crossroads of Astrophysics, ed. R. Cesaroni et al. (Cambridge: Cambridge Univ. Press), 111
Kurtz, S., Cesaroni, R., Churchwell, E., Hofner, P., & Walmsley, C. M. 2000, in Protostars and Planets IV, ed. V. Mannings, A. P. Boss, & S. S. Russell (Tucson, AZ: Univ. of Arizona Press), 299
Laas, J. C., Garrod, R. T., Herbst, E., & Widicus Weaver, S. L. 2011, ApJ, 728, 71
Le Teuff, Y. H., Millar, T. J., & Markwick, A. J. 2000, A&AS, 146, 157
Lee, C. W., Cho, S.-H., & Lee, S.-M. 2001, ApJ, 551, 333
Lefloch, B., Cabrit, S., Busquet, G., et al. 2012, ApJL, 757, L25
Lefloch, B., Cabrit, S., Codella, C., et al. 2010, A&A, 518, L113
Leigh, D., Remijan, A., & Turner, B. 2007, BAAS, 39, 961
Li, J., Wang, J., Gu, Q., yu Zhang, Z., & Zheng, X. 2012, ApJ, 745, 47
Ligterink, N. F. W., Tenenbaum, E. D., & van Dishoeck, E. F. 2015, A&A, 576, A35
Liu, S.-Y., Girart, J. M., Remijan, A., & Snyder, L. E. 2002, ApJ, 576, 255
Liu, S.-Y., Mehringer, D. M., & Snyder, L. E. 2001, ApJ, 552, 654
Loison, J.-C., Agúndez, M., Marcelino, N., et al. 2016, MNRAS, 456, 4101
López-Sepulcre, A., Jaber, A. A., Mendoza, E., et al. 2015, MNRAS, 449, 2438
Loughran, L., McBreen, B., Fazio, G. G., et al. 1986, ApJ, 303, 629
Lykke, J. M., Favre, C., Bergin, E. A., & Jrgensen, J. K. 2015, A&A, 582, A64
Lyo, A.-R., Kim, J., Byun, D.-Y., & Lee, H.-G. 2014, AJ, 148, 80
Macdonald, G. H., Gibb, A. G., Habing, R. J., & Millar, T. J. 1996, A&AS, 119, 333
MacDonald, G. H., Habing, R. J., & Millar, T. J. 1995, Ap&SS, 224, 177
Madden, S., Irvine, W., Swade, D., Matthews, H., & Friberg, P. 1989, AJ, 97, 1403
Mangum, J. G., Wootten, A., Wadiak, E. J., & Loren, R. B. 1990, ApJ, 348, 542
Maret, S., Ceccarelli, C., Caux, E., et al. 2004, A&A, 416, 577
Maret, S., Ceccarelli, C., Tielens, A. G. G. M., et al. 2005, A&A, 442, 527
Margulès, L., Huet, T. R., Demaison, J., et al. 2010, ApJ, 714, 1120
Martí, J., Rodriguez, L. F., & Reipurth, B. 1993, ApJ, 416, 208
Martín-Pintado, J., Rizzo, J. R., de Vicente, P., Rodrguez-Fernández, N. J., & Fuente, A. 2001, ApJL, 548, L65
Matthews, H. E., McCutcheon, W. H., Kirk, H., White, G. J., & Cohen, M. 2008, ApJ, 136, 2083
Maud, L. T., Moore, T. J. T., Lumsden, S. L., et al. 2015, MNRAS, 453, 645
Maxia, C., ti, L. T., aroni, R. C., & ley, C. M. W. 2001, A&A, 371, 287
McKee, C. F., & Tan, J. C. 2003, ApJ, 585, 850
Megeath, S. T., & Tieftrunk, A. R. 1999, ApJL, 526, L113
Mehringer, D. M., Goss, W. M., & Palmer, P. 1995, ApJ, 452, 304
Mehringer, D. M., & Snyder, L. E. 1996, ApJ, 471, 897
Mehringer, D. M., Snyder, L. E., Miao, Y., & Lovas, F. J. 1997, ApJL, 480, L71
Menten, K. M., Walmsley, C. M., Henkel, C., & Wilson, T. L. 1986, A&A, 157, 318
Miao, Y., & Snyder, L. E. 1997, ApJL, 480, L67
Millar, T. J., MacDonald, G. H., & Habing, R. J. 1995, MNRAS, 273, 25
Minh, Y., Chen, H.-R., Su, Y.-N., & Liu, S.-Y. 2012, JKAS, 45, 157
Minh, Y., Ohishi, M., Roh, D., Ishiguro, M., & Irvine, W. M. 1993, ApJ, 411, 773
Minh, Y. C., Su, Y.-N., Chen, H.-R., et al. 2010, ApJ, 723, 1231
Minier, V., & Booth, R. S. 2002, A&A, 387, 179
Mookerjea, B., Casper, E., Mundy, L. G., & Looney, L. W. 2007, ApJ, 659, 447
Morris, P. W., Gupta, H., Nagy, Z., et al. 2016, ApJ, 829, 15
Moscadelli, L., Li, J. J., Cesaroni, R., et al. 2013, A&A, 549, A122
Müller, H., Schlöder, F., Stutzki, J., & Winnewisser, G. 2005, JMoSt, 742, 215
Müller, H. S. P., Thorwirth, S., Roth, D. A., & Winnewiser, G. 2001, A&A, 370, L49
Neckel, T. 1978, A&A, 69, 51
Neill, J. L., Bergin, E. A., Lis, D. C., et al. 2014, ApJ, 789, 8
Nummelin, A., Bergman, P., Hjalmarson, A., et al. 1998a, ApJS, 117, 427
Nummelin, A., Bergman, P., Hjalmarson, A., et al. 2000, ApJS, 128, 213
Nummelin, A., Dickens, J., Bergman, P., et al. 1998b, A&A, 337, 275
Öberg, K. I., Bottinelli, S., Jørgensen, J. K., & van Dishoeck, E. F. 2010, ApJ, 716, 825
Olmi, L., Cesaroni, R., Neri, R., & Walmsley, C. M. 1996a, A&A, 315, 565
Olmi, L., Cesaroni, R., & Walmsley, C. 1995, BAAS, 27, 862
Olmi, L., Cesaroni, R., & Walmsley, C. M. 1993, A&A, 276, 489
Olmi, L., Cesaroni, R., & Walmsley, C. M. 1996b, A&A, 307, 599
Ortega, M. E., Paron, S., Cichowolski, S., Rubio, M., & Dubner, G. 2012, A&A, 546, A96
Osorio, M., Anglada, G., Lizano, S., & D'Alessio, P. 2009, ApJ, 694, 29
Pandian, J. D., Momjian, E., & Goldsmith, P. F. 2008, A&A, 486, 191
Pankonin, V., Churchwell, E., Watson, C., & Bieging, J. H. 2001, ApJ, 558, 194
Parise, B., Ceccarelli, C., Tielens, A. G. G. M., et al. 2006, A&A, 453, 949
Pascucci, I., Apai, D., Henning, T., Stecklum, B., & Brandl, B. 2004, A&A, 426, 523
Peng, T. C., Despois, D., Brouillet, N., et al. 2013, A&A, 554, A78
Persi, P., Marenzi, A. R., Tapia, M., & Bohigas, J. 2003, MmSAI, 74, 146
Persi, P., Tapia, M., & Roth, M. 2000, A&A, 357, 1020
Persson, C. M., Olofsson, A. O. H., Koning, N., et al. 2007, A&A, 476, 807
Pickett, H. M., Poynter, R. L., Cohen, E. A., et al. 1998, JQSRT, 60, 883
Pipher, J. L., Soifer, B. T., & Krassner, J. 1979, A&A, 74, 302
Plambeck, R. L., & Menten, K. M. 1990, ApJ, 364, 555
Plume, R., Fuller, G. A., Helmich, F., et al. 2007, PASP, 119, 102
Purcell, C. R., Balasubramanyam, R., Burton, M. G., et al. 2006, MNRAS, 367, 553
Qin, S.-L., Schilke, P., Wu, J., et al. 2015, ApJ, 803, 39
Qin, S.-L., Wu, Y., Huang, M., et al. 2010, ApJ, 711, 399
Qiu, K., & Zhang, Q. 2009, ApJL, 702, L66
Rad, M. L., Zou, L., Sanders III, J. L. S., & Widicus Weaver, S. L. 2016, A&A, 585, A23
Raimond, E. 1966, BAN, 18, 191
Ratajczak, A., Taquet, V., Kahane, C., et al. 2011, A&A, 528, L13
Rathborne, J. M., Garay, G., Jackson, J. M., et al. 2011, ApJ, 741, 120
Reiter, M., Shirley, Y. L., Wu, J., et al. 2011, ApJS, 195, 1
Remijan, A., Shiao, Y.-S., Friedel, D. N., Meier, D. S., & Snyder, L. E. 2004a, ApJ, 617, 384
Remijan, A., Snyder, L. E., Friedel, D. N., Liu, S.-Y., & Shah, R. Y. 2003, ApJ, 590, 314
Remijan, A., Snyder, L. E., Liu, S.-Y., Mehringer, D., & Kuan, Y.-J. 2002, ApJ, 576, 264
Remijan, A., Sutton, E. C., Snyder, L. E., et al. 2004b, ApJ, 606, 917
Remijan, A. J., Leigh, D. P., Markwick-Kemper, A. J., & Turner, B. E. 2008, arXiv:0802.2273
Requena-Torres, M. A., Marcelino, N., Jiménez-Serra, I., et al. 2007, ApJL, 655, L37
Requena-Torres, M. A., Martín-Pintado, J., Rodríguez-Franco, A., et al. 2006, A&A, 455, 971
Rice, F., Sumner, M., Zmuidzinas, J., et al. 2003, Proc. SPIE, 4855, 301
Richardson, K. J., Sandell, G., Cunningham, C. T., & Davies, S. R. 1994, A&A, 286, 555
Riffel, R. A., & Lüdke, E. 2010, MNRAS, 404, 1449
Rolffs, R., Schilke, P., Zhang, Q., & Zapata, L. 2011, A&A, 536, A33
Rosero, V., Hofner, P., Kurtz, S., Bieging, J., & Araya, E. D. 2013, ApJS, 207, 12
Sakai, N., Ceccarelli, C., Bottinelli, S., Sakai, T., & Yamamoto, S. 2012, ApJ, 754, 70
Sakai, N., Sakai, T., Hirota, T., Burton, M., & Yamamoto, S. 2009a, ApJ, 697, 769
Sakai, N., Sakai, T., Hirota, T., & Yamamoto, S. 2008, ApJ, 672, 371
Sakai, N., Sakai, T., Hirota, T., & Yamamoto, S. 2009b, ApJ, 702, 1025
Sakai, N., Sakai, T., & Yamamoto, S. 2006, PASJ, 58, L15
Sakai, N., Sakai, T., & Yamamoto, S. 2007, ApJ, 660, 363
Sánchez-Monge, A., Kurtz, S., Palau, A., et al. 2013, ApJ, 766, 114
Saruwatari, O., Sakai, N., Liu, S.-Y., et al. 2011, ApJ, 729, 147

Sato, M., Reid, M. J., Brunthaler, A., & Menten, K. M. 2010, ApJ, 720, 1055
Schilke, P., Benford, D. J., Hunter, T. R., Lis, D. C., & Phillips, T. G. 2001, ApJS, 132, 281
Schilke, P., Groesbeck, T. D., Blake, G. A., & Phillips, T. G. 1997, ApJS, 108, 301
Schneider, N., Bontemps, S., Simon, R., et al. 2006, A&A, 458, 855
Scoville, N. Z., Sargent, A. I., Sanders, D. B., et al. 1986, ApJ, 303, 416
Shi, H., Zhao, J.-H., & Han, J. L. 2010, ApJ, 710, 843
Shirley, Y. L., Evans II, N. J., Rawlings, J. M. C., & Gregersen, E. M. 2000, ApJS, 131, 249
Slysh, V. I., Kalenskii, S. V., & Val'tts, I. E. 2002, ARep, 46, 49
Slysh, V. I., Kalenskii, S. V., Val'tts, I. E., Golubev, V. V., & Mead, K. 1999, ApJS, 123, 515
Snyder, L. E. 2006, PNAS, 103, 12243
Snyder, L. E., Lovas, F. J., Mehringer, D. M., et al. 2002, ApJ, 578, 245
Stark, R., van der Tak, F. F. S., & van Dishoeck, E. F. 1999, ApJL, 521, L67
Straizys, V., Cernis, K., Kazlauskas, A., & Meistas, E. 1992, BaltA, 1, 149
Straw, S. M., Hyland, A. R., & McGregor, P. J. 1989, ApJS, 69, 99
Sumner, M. C. 2011, PhD thesis, California Institute of Technology
Sutton, E. C., Blake, G. A., Masson, C. R., & Phillips, T. G. 1985, ApJS, 58, 341
Sutton, E. C., Peng, R., Danchi, W. C., et al. 1995, ApJS, 97, 455
Sutton, E. C., Sobolev, A. M., Salii, S. V., et al. 2004, ApJ, 609, 231
Suzuki, T., Ohishi, M., Hirota, T., et al. 2016, ApJ, 825, 79
Tahani, K., Plume, R., Bergin, E. A., et al. 2016, ApJ, 832, 12
Taquet, V., López-Sepulcre, A., Ceccarelli, C., et al. 2015, ApJ, 804, 81
Thorwirth, S., Walsh, A. J., Wyrowski, F., et al. 2007, in Molecules in Space and Laboratory, ed. J. L. Lemaire & F. Combes (Paris: S. Diana), 39
Tobin, J. J., Looney, L. W., Wilner, D. J., et al. 2015, ApJ, 805, 125
Turner, B. E. 1989, ApJS, 70, 539
Turner, B. E. 1991, ApJS, 76, 617
Turner, J. L., & Welch, W. J. 1984, ApJL, 287, L81
van der Tak, F. F. S., van Dishoeck, E. F., & Caselli, P. 2000, A&A, 361, 327
van Dishoeck, E. F., Kristensen, L. E., Benz, A. O., et al. 2011, PASP, 123, 138
Vig, S., Cesaroni, R., Testi, L., Beltrán, M. T., & Codella, C. 2008, A&A, 488, 605
Wakelam, V., Caselli, P., Ceccarelli, C., Herbst, E., & Castets, A. 2004, A&A, 422, 159
Wakelam, V., Ceccarelli, C., Castets, A., et al. 2005, A&A, 437, 149
Walmsley, C. M., Cesaroni, R., Olmi, L., Churchwell, E., & Hofner, P. 1995, Ap&SS, 224, 173
Walsh, A. J., Thorwirth, S., Beuther, H., & Burton, M. G. 2010, MNRAS, 404, 1396
Ward-Thompson, D., Zylka, R., Mezger, P. G., & Sievers, A. W. 2000, A&A, 355, 1122
Watanabe, Y., Sakai, N., López-Sepulcre, A., et al. 2015, ApJ, 809, 162
Watson, C., Churchwell, E., Pankonin, V., & Bieging, J. H. 2002, ApJ, 577, 260
Watt, S., & Mundy, L. G. 1999, ApJS, 125, 143
Werner, M. W., Becklin, E. E., Gatley, I., et al. 1979, MNRAS, 188, 463
White, G. J., Araki, M., Greaves, J. S., hi, M. O., & Higginbottom, N. S. 2003, A&A, 407, 589
Willner, S. P. 1976, ApJ, 206, 728
Wilner, D. J., Reid, M. J., & Menten, K. M. 1999, ApJ, 513, 775
Wilner, D. J., Welch, W. J., & Forster, J. R. 1995, ApJL, 449, L73
Wirström, E. S., Geppert, W. D., Hjalmarson, A., et al. 2011, A&A, 533, A24
Wood, D. O. S., & Churchwell, E. 1989, ApJS, 69, 831
Wootten, A., & Mangum, J. 2009, in ASP Conf. Ser. 417, Submillimeter Astrophysics and Technology: a Symposium Honoring Thomas G. Phillips, ed. D. C. Lis et al. (San Francisco, CA: ASP), 219
Wu, J., II, N. J. E., Shirley, Y. L., & Knez, C. 2010, ApJS, 188, 313
Wu, Y., Qin, S.-L., Guan, X., et al. 2009, ApJL, 697, L116
Wyrowski, F., Hofner, P., Schilke, P., et al. 1997, A&A, 320, L17
Wyrowski, F., Schilke, P., & Walmsley, C. M. 1999a, A&A, 341, 882
Wyrowski, F., Schilke, P., Walmsley, C. M., & Menten, K. M. 1999b, ApJL, 514, L43
Zapata, L. A., Loinard, L., Su, Y.-N., et al. 2012, ApJ, 744, 86
Zapata, L. A., Schmid-Burgk, J., & Menten, K. M. 2011, A&A, 529, A24